OFDM/OQAM based terrestrial digital broadcasting

Anahita Goljahani

University of Padova, faculty of Engineering

Department of Information Engineering

Ph.D. School in Information Engineering, XXI cycle

Electronic and Telecommunications Engineering

Head: Ch.mo Prof. M. Bertocco
Supervisor: Ch.mo Prof. L. Vangelista
Doctoral candidate: Anahita Goljahani

A te, zia, sempre.

A te, Fede: in queste pagine la tua generosità, la tua intelligenza, la tua pazienza.

Alla mia famiglia e a chi continua a salvarmi giorno dopo giorno.

Acknowledgements

Ringrazio tutti coloro che hanno contribuito alla mia formazione.
Ringrazio il Prof. Vangelista per avermi sostenuta e guidata, indossando a volte la veste di supervisore, a volte la veste di amico.
Ringrazio il Prof. Pupolin per aver avuto fiducia in me e aver permesso che questo percorso iniziasse.

Abstract

In this thesis an OFDM/ OQAM based system for the next generation terrestrial digital broadcasting standard is proposed and its performance, in terms of spectral efficiency, is compared to OFDM-CD3 performance. As far as coding is concerned, LDPC and BCH codes have been utilized, synchronization and channel estimation have been performed by a superimposed technique and a one tap MMSE equalization scheme has been adopted. As shown by simulation results, an improvement of more than 13% is achieved by OFDM/OQAM system, confirming, in a practical system, the expectation of a significant spectral efficiency improvement.

Contents

List of Figures

Nomenclature

Symbols

$\mathcal{A}$ Active indexes set: $\{i_a : 0 \leq i_a \leq \lfloor \frac{N_a}{2} \rfloor \text{ or } M - \lfloor \frac{N_a}{2} \rfloor \leq i_a \leq M-1\}$

β Fraction of $\sigma^2_{s_u}$ assigned to $p_{sup}(k)$

Δ Fraction of OFDM symbol assigned to the cyclic prefix

F Transmission rate

$T\ (= \frac{1}{F})$ Elementary period/Sampling period

F_0 Staggered stream rate/Data rate

F_1 PN sequence rate

$T_1\ (= \frac{1}{F_1})$ PN sequence sampling period

F_s Baud rate/Symbol rate

F_u CD3-OFDM subcarriers distance

$T_u\,(F_u^{-1})$ MT

$H(f)$ Channel frequency response

$\mathbf{H}_a$ Vector of CFR values on active subcarriers frequencies

h(kT) Channel impulse response

$\mathfrak{I}(t)$ prototype function of the IOTA transform

j Imaginary unit

L Filter length

L_h CIR length

$L_{p'_n}$ PN sequence period

L_{p_n} Rate converted PN sequence period

M Subcarriers number

N $\frac{M}{2}$

N_a Active subcarriers number

N_{CP} CP length

N_{sup} N_{sup} is such that $L_{pn} = N_{sup}M$

N_V Number of virtual carriers

$p_n^t(kT)$, $p_n'^t(kT_1)$ See defintions (2.6)

$p_n(kT)$ Rate converted sequence

$p'_n(kT_1)$ PN sequence

$r_h(kT)$ Received signal

$r_h^{(sup)}(kT)$ Superimposed received signal

$r_h^{(s_u)}(kT)$ Useful received signal

$r_x(\nu' T_s)$ autocorrelation of $x(n'T_s)$

$r_{x,y}(\nu' T_s)$ crosscorrelation between $x(n'T_s)$ and $y(n'T_s)$

σ_w^2 System noise power

$\sigma^2_{r_h^{(s_u)}}$ $r_h^{(s_u)}$ power

$\sigma^2_{r_h^{(sup)}}$ $r_h^{(sup)}$ power

$\sigma^2_{s_u}$ Average $s_u(k)$ power/Useful power

$\sigma^2_{p_{sup}}$ p_{sup} power

$s_u(k)$ Modulated signal/useful signal

T_0 $(= \frac{1}{F_0})$ Staggered stream sampling period

T_s $(= \frac{1}{F_s})$ OFDM symbol duration

$u_b(nT_0)$ Output of the demodulator corresponding to branch b

$w(kT)$ System noise

$\mathbf{x}_a$ Vector containing ordered active subcarriers indexes

Operators

$\cong$ Almost equal

$*$ Convolution operator

$\delta(\cdot)$ Kronecker delta

E$[\cdot]$ Expectation operator

./ Element wise division

.$*$ Element wise multiplication

$Im[\cdot]$ Imaginary part

$\lfloor x \rfloor$ Returns the greater integer less or equal to x

$\uparrow N$ Interpolation by N

$|\cdot|$ Absolute value operator

mod Module operator: $a \mod b = a - \lfloor \frac{a}{b} \rfloor b$

$Re[\cdot]$ Real part

$\downarrow N$ Sampling by N

$\triangleq$ Definition

$'$ Transpose conjugate

^{T} Transpose operator.

$\cup$ Sets union operator

$\mathbf{v}[i]$ ith element of the vector $\mathbf{v}$

Acronyms

BER Bit Error Rate

CD3 Coded Decision Directed Demodulation

CFR Channel Frequency Response

CIR Channel Impulse Response

COFDM Coded Orthogonal Frequency Division Multiplexing

CP Cyclic Prefix

CP-OFDM Cyclic Prefix-OFDM

DAB Digital Audio Broadcasting

DAC Digital to Analog Converter

DFT Discrete Fourier Transform

DVB-C Cable Digital Video Broadcasting

DVB Digital Video Broadcasting project

DVB-S2 Second generation DVB-S

DVB-S Satellite Digital Video Broadcasting

DVB-T2 new generation Terrestrial Digital Video Broadcasting

DVB-T Terrestrial Digital Video Broadcasting

ETSI European Telecommunications Standards Institute

FEC Forward Error Correction

FR Frequency response

HDTV High Definition Television

IDFT Inverse Discrete Fourier Transform

i.i.d. Independent Identically Distributed

IOTA Isotropic Orthogonal Transform Algorithm

LDPC Low Density Parity Check

LMMSE Linear Minimum Mean Square Equalizer

MSE Mean Square Error

OFDM-CD3 Coded Decision Directed Demodulation OFDM

OFDM Orthogonal Frequency Division Multiplexing

OFDM/OQAM Orthogonal Frequency Division Multiplexing /Offset Quadrature amplitude Modulation

OQAM Offset QAM

PN Pseudo Noise

POP Pair of Pilots

PSD Power Spectral Density

S/P Serial to Parallel conversions

SNR Signal to Noise Ratio, see def. (2.10)

SNR_{eq} Equivalent Signal to Noise Ratio, see def. (2.11)

ZF Zero Forcing

Chapter 1

Introduction

Technological progress and ever increasing demand of higher quality services has driven the digitalization of broadcasting networks since the 1990's. Researchers have focused on finding an efficient basedand digital coding, combined with a robust digital modulation and channel coding scheme. To this aim, the coded orthogonal frequency division multiplexing (COFDM) technology has been under study both for digital audio broadcasting (DAB) and digital video broadcasting [1] . In the field of DAB, the work has been completed at the end of the 80's [2]. Digital video broadcasting standardization has been supported and developed by the Digital Video Broadcasting project (DVB) [3], an industry-led consortium of over 270 broadcasters constituted in 1993. The technical specifications approved by the DVB are submitted to the Euro pean Telecommunications Standards Institute (ETSI) , whose ratification make them official European standards. The specifications for the satellite multi-programm TV transmission (DVB-S) [4] have been the first important result achieved by DVB, followed by the specifications for the cable multi-programme TV distribution (DVB-C) [5] . However, due to the large number of users of the television services consumers, results obtained in the field of the terrestrial digital video broadcasting (DVB-T) are the most important. The main issues to deal with were the transmission in the terrestrial VHF/UHF bands, the congestion of the television frequency spectrum, the

deployment of single frequency networks (SFN). The first DVB-T specifications have been completed at the end of 1995 and approved by ETSI in 1997 [6]. The terrestrial channel is characterized by a multi-path propagation, due to natural echoes (reflections and diffractions by different kind of obstacles) or artificial echoes (signals coming from isofrequential transmitters), that causes a heavy distortion of the transmitted signal. In the presence of such a channel, the use of a single carrier modulation would require a complicated and long equalizer. Hence, COFDM, successfully applied in DAB, has been adopted also in DVB-T. Since its publication, DVB-T has enjoyed a great success, becoming the most popular way to distribute TV in Europe and in many other parts in the world. However, the introduction of MPEG4 and DVB-S2 [7], driving the first adoption of High Definition TV (HDTV) on satellite and cable networks, has pointed out the limit of the DVB-T standard in supporting higher transmission rates. In 2006, then, the terrestrial TV broadcasting community began working on the improvement of the DVB-T standard, aiming at defining a system providing a minimum of 30% capacity increase over DVB-T. The specifications of the new generation terrestrial digital video broadcasting (DVB-T2) are summarized in the document published by DVB project in June 2008 [8], sent to ETSI for standardization. The efficiency improvement of $30 - 50\%$ achieved in the use of the spectrum makes DVB-T2 based systems capable to offer HDTV services. The same basic modulation technique as DVB-T, namely cyclic-prefix OFDM (CP-OFDM), with an extended range of FFT size, guard intervals and constellations, has been adopted by DVB-T2. Moreover, baseband framing and forward-error-correction processes are the same as the second-generation satellite broadcasting system DVB-S2 [7]. The high performance promised by the DVB-T2 and the need of ever higher transmission rates have made an attractive challenge to develop a comprehensive DVB-T2 like system, involving coding, channel estimation, frame synchronization, equalization, based on a modulation technique always addressed as the alternative to the CP-OFDM which would have *theoretically* provided a better spectral efficiency, namely the Orthogonal Frequency Division Multiplexing/Offset

Quadrature Amplitude Modulation (OFDM/OQAM) [1]. In this thesis a proposal and analysis of such a kind of system is presented, confirming the high potentials of OFDM/OQAM. As explained in the following, the main effort has been made on channel estimation and synchronization task. Indeed, the novelty of estimating the channel in an OFDM/OQAM system through the superimposed correlation-based method [9] is presented in this thesis, along with the analysis of the possibility of exploiting the same superimposed pseudo noise (PN) sequence for symbol synchronization purposes.

OFDM/OQAM is a multichannel system where parallel data transmission is achieved by independently modulating a number of carriers spaced a baud rate apart. Avoiding spectral overlap of the channels is one way to eliminate interchannel interference. However, this may lead to inefficient use of the available spectrum. Higher overall signaling rates can be achieved if spectral overlap is permitted, and some orthogonality relationship is used to minimize the interference between adjacent channels. In 1966 Chang [10] presented general conditions under which *bandlimited* channels, each carrying a *complex* data rate of F_s, may be spaced F_s apart in frequency with no resultant intersymbol or interchannel interference. The first published parallel data transmission system, meeting Chang's conditions, and the analysis of its performance over a dispersive transmission medium have been presented by Saltzberg [11] in 1967. The system has been addressed as the first orthogonally multiplex QAM system [12]. In the proposed scheme, parallel *real* data streams were conveyed, at a rate of $2F_s$, through channels with identical spectral shaping given by full roll-off square root raised cosine pulses, spaced F_s apart. In order to avoid interchannel interference, adjacent channels were in phase quadrature. The proposal of a discrete Fourier transform (DFT) based digital implementation of OFDM/OQAM system, by Hirosaki [12], was followed by further efficient schemes presented by Cariolaro [13] and Siohan [14]. Once identified fast implementations, the research on OFDM/OQAM has been lot focusing on the finding of prototype filters obeying the OFDM/OQAM

prerequisites. To remove the guard interval, used by the classical OFDM, denoted hereinafter as CP-OFDM, the prototype function modulating each subcarrier must be very well localized both in the time and in the frequency domain, in order to efficiently combat the multi-path effect and limit the inter-symbol and interchannel interferences. Moreover, this function must also guarantee orthogonality between sub-carriers. To this aim, in [1], the authors have presented an orthogonalization algorithm called isotropic orthogonal transform algorithm (IOTA) , namely a two step orthogonalization algorithm, attributed to Henri Poincaré, applied to the Gaussian functions. This procedure provides well localized time-frequency prototype functions [15]. Among them, the one which leads to a perfect symmetry between the time and frequency axis is called prototype function of the IOTA transform and is denoted by $\mathfrak{I}(t)$. Its localization measure is very close to the optimal [16]. Orthogonality conditions on prototype filters have been presented for some times only on continuous time pulses of infinite length. However a natural consequence of a DFT-based implementation is the truncation and discretization of the pulse shape, causing a loss of orthogonality. In [14] conditions of discrete orthogonality have been established with respect to the polyphase components of the prototype filter, assumed to be symmetrical and with arbitrary length. Infinite length, discretized $\mathfrak{I}(t)$ function satisfies discrete orthogonality conditions [16]. Although analytical results derived in the subsequent chapters are valid for any prototype filter satisfying orthogonality conditions, final results, based on simulations, are obtained utilizing the discrete *truncated* $\mathfrak{I}(t)$ prototype filter. Due to the truncation, orthogonality conditions are no more satisfied, but experimental results show that the system achieves high efficiency level with a filter length L equal to $L = 4M$, where M is the number of subcarriers.

The drawback of the OFDM/OQAM system is an *intrinsic* inter symbol interference [17], due to the fact that orthogonality conditions hold only on the *real* field. Hence, classical OFDM/QAM channel estimation methods cannot be directly applied to OFDM/OQAM based systems. Solutions have been proposed

for preamble based channel estimation in [18], [19] and [20]. Results concerning the performance of the estimation technique presented in [20] show a gain of 2 dB with respect to the CP-OFDM for an IEEE802.22 channel model. However,the proposed preamble based estimation technique requires the hypothesis of a static channel, that is not the case of many wireless scenarios. Scattered-based channel estimations for OFDM/OQAM have also been presented in [17] and [19]. In [19] a technique denoted as pair of pilots (POP) has been proposed. Unfortunately, POP performance is poor, as reported in [19]. In [17], the authors propose to cancel the first order intrinsic interference by determining one of the 8 first order neighbor sub-carriers of the scattered pilot by the others. The drawback is that the computed value doesn't belong to the transmitted constellation, forcing to apply some mathematical relation to evenly distribute their energy.

As already anticipated, to overcome the effect of the intrinsic interference and preserve the promised increase in spectral efficiency, the novelty of estimating the channel through the superimposed correlation-based method [9] is presented in this thesis. The technique has already been studied for the CP-OFDM system [21], but never applied to OFDM/OQAM based systems. In this thesis the case of spectrum mask constraints, which prevents the technique from being directly applied, has been analyzed. Indeed, conventional superimposed correlation method is based on the straightforward superposition of a low power pseudo noise (PN) sequence to the useful transmitted signal and the recovery of the channel values through a filtering by the matched PN sequence. Unfortunately, the white spectrum of the PN sequence may not fulfill realistic spectrum mask constraints, forcing to a rate conversion before the superposition, as is the case of the specifications considered in this work. The convenience of exploiting the *rate converted* superimposed sequence for symbol synchronization purpose is also studied in this thesis. In [22], clock, symbol, frequency and frame synchronization are obtained by a complex time correlation between the modulated received signal and the time representation of the scattered pilots sequence. The authors assume that the transmitted frame is structured as a typical CP-OFDM frame

with subcarriers reserved for insertion of known pilots (scattered pilots) dedicated to channel estimation purposes. However, from the previous considerations about channel estimation techniques, it doesn't seam a proper assumption. As far as equalization is concerned in OFDM/OQAM based systems, an interference cancelation method has been recently proposed in [23], aiming at avoiding performance floor noticed when a zero forcing (ZF) equalization is used for channels with large delay spread and/or when using higher order constellations. The system proposed in this thesis includes per branch linear equalizers with coefficients computed according to the minimum mean square error criterion (MMSE) [24]. For the 16k operational mode (16384 subcarriers) of the DVB-T2 [8] standard and the fixed rooftop reception channel, considered in this thesis, one tap equalization has showed to be the proper solution. Equalizers coefficients computation requires the knowledge of the system noise power σ_w^2 , unknown at the receiver side. An interference cancelation loop is presented in this thesis in order to estimate σ_w^2. Equalization performance presented in [24] are based on the perfect channel knowledge, which is not the case of the system proposed in this thesis. The effectiveness of the technique combined with the proposed channel estimation technique has been validated through simulation results. As far as the encoding part of the proposed scheme is concerned, all the specifications are based on DVB-T2 forward error correction (FEC) encoding, which consists of a concatenation of t-error correcting BCH outer code and low density parity check (LDPC) inner code [8].

The aim of this work is to analyze, through experimental results, the functionality of the *whole* system, rather than focusing on theoretical results regarding single blocks, often based on the unrealistic hypothesis of ideal conditions, never satisfied in practise. The performance of the system is measured in terms of achievable throughput (*useful* bit rate at BER=10^{-6}) per Hz. We will refer to this quantity as spectral efficiency. As a means of comparison, spectral efficiency of coded decison directed demodulation OFDM (OFDM-CD3) based system [25] is also derived. The channel estimation scheme presented in [25] is based on a

channel estimation loop exploiting the error correction capability of a FEC decoder. Although DVB-T2 standard provides for 8 pilot patterns, OFDM-CD3 has been addressed as, since it does not require the transmission of a comb of pilot tones, it is one of the best in terms of spectral efficiency, yielding an improvement between 5% to 15% [25].

This work is an effort towards the *practical* realization of an OFDM/OQAM based system. Indeed, technology and architecture enhancements, allowing much more Digital Signal Processing (DSP) operations with the same, or even lower, power consumption and silicon area, have made OFDM/OQAM a technology whose feasibility can be seriously considered.

The thesis is organized as follows. An overview of both OFDM/OQAM and CD3-OFDM based systems is given in Chapter 2, in order to highlight the interaction between the building blocks and give comprehensive reference schemes to facilitate the understanding of the subsequent development. In Chapter 3 system specifications are introduced, from coding to channel model. Indeed, since results are mainly based on simulations, references to environment specifications are necessary throughout the development of the whole thesis. In Chapter 4 the discrete baseband OFDM/OQAM is introduced. Based on the formulation of the demodulated signal, quantities related to the prototype filter needed for the analysis of the interference and the equalization task are identified and computed. Moreover, the number of active subcarriers is computed, in order to transmit a signal with a spectrum satisfying limitations given by the mask specification and clearly quantify the gain achieved thanks to the better frequency localization of the $\mathcal{I}(t)$ pulse shape with respect to the rectangular pulse shape used in CP-OFDM. In Chapter 5 the superimposed channel estimation technique is presented. The rate-converter needed to satisfy mask constraints is also presented and performance results in terms of per carrier mean square error (MSE) are given for superimposed sequence powers corresponding to the optimum ones. Results validating the opportunity of exploiting the superimposed *rate converted* sequence for synchronization purposes are also presented. Chapter 6 is dedicated

to the linear minimum mean square equalization formulation and analysis. In [24] a frequency domain approach have been presented to compute equalization coefficients. In this thesis a time domain approach, based on the quantities introduced in Chapter 4, is utilized. The interference cancelation loop for noise power estimation is also described. In Chapter 7 results in terms of spectral efficiency of both the system proposed in this thesis and the CD3-OFDM are presented.

Chapter 2

OFDM/OQAM and CD3-OFDM systems overview

In this chapter high level block diagrams of both OFDM/OQAM and CD3-OFDM systems are presented. A first description of blocks functionality is provided in order to highlight interactions between main parts of the systems and supply a comprehensive reference scheme supporting the insight given in subsequent chapters. Most of the notations and definitions utilized hereinafter are also introduced.

2.1 OFDM/OQAM system

Fig. 2.1 shows the high level block diagram of the discrete baseband equivalent of the OFDM/OQAM system.

An incoming bit-stream feeds a first functional block which performs the forward error correction (FEC) encoding, given by the concatenation of a BCH and LDPC code. Then, bit interleaving, multiplexing and mapping to QAM constellation are performed. These operations are better specified in Chapter 3. The resulting stream is filled with zeros in positions corresponding to the virtual subcarriers, in order to suitably shape the spectrum of the transmitted signal. Data bearing subcarriers are addressed as *active* subcarriers and their number is denoted by N_a. The rate of the resulting signal is defined as *transmission rate* and

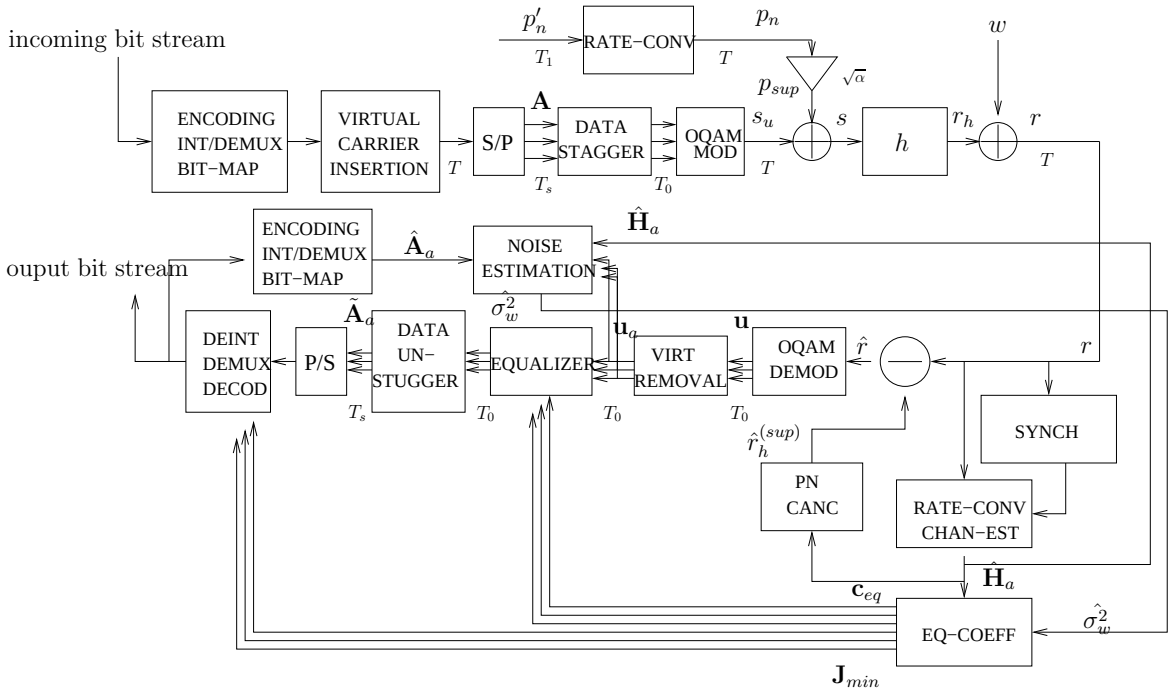

Figure 2.1: High level OFDM/OQAM system block diagram.

is denoted by F. Its inverse, $T = 1/F$, is called *elementary period* or *sampling period*. Serial to parallel conversion, denoted by S/P , produces M low rate QAM symbols streams, where M is the number of system subcarriers. Low rate QAM streams are denoted by the vectorial function $\mathbf{A}(n'T_s)$, whose bth component, corresponding to bth branch stream, is denoted by $A_b(n'T_s)$. The set of values assumed by $\mathbf{A}(n'T_s)$ at any instant $n'T_s$ is called OFDM symbol. T_s is called OFDM symbol duration and corresponds to the time required to transmit one OFDM symbol. $F_s = T_s^{-1}$ is called *baud rate* or *symbol rate*. The staggering operation consists in splitting the incoming low rate QAM symbols in their real and imaginary part, yielding a double rate, $F_0 = 2F_s$, real stream, defined as *data* stream. F_0 is defined as data rate and its inverse is denoted by $T_0 = 1/F_0$. Operations performed on data streams to produce the modulated signal $s_u(kT)$ are called OQAM modulation. Namely, M subcarriers, spaced F_s apart, are modulated by the data streams filtered by a prototype filter satisfying OQAM

orthogonality conditions, e.g. $\mathcal{I}(t)$ function. Only N_a subcarriers are active and the set of indexes

$$\mathcal{A} \triangleq \{i_a : f_{i_a} = i_a F_s \text{ is the frequency of an active subcarrier}\} \tag{2.1}$$

is called *active* indexes set. Here

$$\mathcal{A} = \{i_a : \{0 \leq i_a \leq \lfloor \frac{N_a}{2} \rfloor\} \cup \{M - \lfloor \frac{N_a}{2} \rfloor \leq i_a \leq M-1\}\} \tag{2.2}$$

where $\lfloor x \rfloor$ is the operator that returns the greater integer less or equal to x and $\cup$ is the sets union operator. The N_a length vector containing the *ordered* indexes belonging to $\mathcal{A}$ is also introduced. It is denoted by

$$\mathbf{x}_a \triangleq \quad \left[0, 1, \ldots, \lfloor \frac{N_a}{2} \rfloor, M - \lfloor \frac{N_a}{2} \rfloor, \ldots, M-1\right] \tag{2.3}$$

and $\mathbf{x}_a[i]$ denotes the ith element of the vector. In general, vectors are denoted in boldface and, given the vector $\mathbf{v}$, by $\mathbf{v}[i]$ is addressed the ith element. To address QAM symbols modulating active subcarriers, the N_a dimensional vectorial function $\mathbf{A}_a(n'T)$ is introduced, whose ith component, $\mathbf{A}_{a,i}(n'T)$, is defined as follows

$$\mathbf{A}_{a,i}(n'T) \triangleq \mathbf{A}_{\mathbf{x}_a[i]}(n'T). \tag{2.4}$$

The modulated signal $s_u(kT)$, defined as *useful* signal, is a ciclostationary random process whose sampling rate is equal to the transmission rate F. Its power, averaged over the ciclostationary period, is denoted by $\sigma^2_{s_u}$ and called *useful* power. A low power sequence $p_{sup}(kT)$ is superimposed to the useful signal $s_u(k)$. $p_{sup}(k)$ is obtained by the scaling of $p_n(kT)$, which is the result of the rate conversion of a CAZAC PN sequence [9], denoted by $p'_n(kT_1)$. $p_n(kT)$ is called *rate converted* sequence. The rate and the sampling period of $p'_n(kT_1)$ are denoted by F_1 ($< F$) and $T_1 = F_1^{-1}$, respectively. The rate conversion ensures that the transmitted signal complies with spectrum mask requirements [26] specified in order to reduce spectral overlapping between transmission signals generated by different transmitters. The scaling factor $\sqrt{\alpha}$, applied to the rate converted sequence $p_n(kT)$,

determines the power of $p_{sup}(k)$, denoted by $\sigma^2_{p_{sup}}$. Since the development is in terms of *fraction* of the useful power assigned to $p_{sup}(k)$, the parameter β is introduced. β is related to α through the relation

$$\sigma^2_{p_{sup}} = \alpha\sigma^2_{p_n} = \beta\sigma^2_{s_u}. \tag{2.5}$$

β is a crucial parameter not only for the estimation and synchronization performance, but also for the whole system efficiency. Indeed, increasing of β on the one hand improves estimation performances, on the other hand degrades the *equivalent* signal to noise ratio, which is defined in (2.11). Hence, it is worthwhile increasing β if the estimation improvement overcomes the equivalent signal to noise decreasing. In this thesis three β values are reported, each corresponding to the best experimentally verified performance for the three constellations provided by the DVB-T2 standard [8], namely $16QAM$, $64QAM$, $256QAM$. The PN sequence $p'_n(kT_1)$ and the rate converted $p_n(kT)$ are periodic signals whose periods are denoted by $L_{p'_n}$ and L_{p_n}, respectively. Two signals, $P'_n(kT_1)$ and $P_n(kT)$, utilized at the receiver side, are here introduced, since their definition is strictly tied to $p'_n(kT_1)$ and $p_n(kT)$

$$\begin{aligned} p'^t_n(kT_1) &= \begin{cases} p'_n(-kT) & \text{for} \quad 0 \le k \le L_{p'_n} - 1 \\ 0 & otherwise \end{cases} \\ p^t_n(kT) &= \begin{cases} p_n(kT) & \text{for} \quad 0 \le k \le L_{p_n} - 1 \\ 0 & otherwise \end{cases} \end{aligned} \tag{2.6}$$

The signal obtained by the superposition of $s_u(kT)$ and $p_{sup}(kT)$, denoted by $s(kT)$, is transmitted through the time and frequency selective channel, whose impulse response (CIR) is denoted by $h(kT)$ and whose channel frequency response (CFR) is denoted by $H(f)$. The CIR average energy is normalized to 1, namely $\mathrm{E}[\sum_{\mathrm{k=0}}^{\mathrm{L_h}-1} |\mathrm{h(k)}|^2] = 1$, where E[ ] is the expectation operator and L_h is the channel length. The M length vector $\mathbf{H}$ is also introduced, whose ith element $\mathbf{H}[i]$ is defined as

$$\mathbf{H}[i] = H(iF_s), \quad i = 0, \ldots, M-1. \tag{2.7}$$

The channel model used for the simulations is specified in Chapter 3.
The received signal $r_h(kT)$ consists of a part due to the channel filtering of $s_u(kT)$, denoted by $r_h^{(s_u)}(kT)$ and called *useful received signal*, and a part due to $p_{sup}(kT)$, denoted by $r_h^{(sup)}(kT)$ and called *superimposed received signal*. Alltogether

$$r_h(kT) = r_h^{(s_u)}(kT) + r_h^{(sup)}(kT). \tag{2.8}$$

Due to the channel energy normalization, the following relations hold

$$\begin{aligned} \sigma^2_{r_h^{(s_u)}} &= \sigma^2_{s_u} \\ \sigma^2_{r_h^{(sup)}} &= \sigma^2_{p_{sup}} \end{aligned} \tag{2.9}$$

where $\sigma^2_{r_h^{(s_u)}}$ and $\sigma^2_{r_h^{(sup)}}$ denote the statistical powers of $r_h(kT)$ and $r_h^{(sup)}(kT)$.
The system noise $w(kT)$, is modeled as a discrete independent identically distributed zero mean circularly symmetric Gaussian random process [9]. Namely every sample is a complex valued Gaussian random variable whose real and imaginary part are uncorrelated and have the same power. The power of $w(k)$ is denoted by σ_w^2. The system signal to noise ratio SNR is defined as follows

$$SNR \triangleq \frac{\sigma^2_{r_h}}{\sigma_w^2} = \frac{\sigma^2_{r_h^{(s_u)}} + \sigma^2_{r_h^{(sup)}}}{\sigma_w^2} = \frac{(1+\beta)\sigma^2_{s_u}}{\sigma_w^2} \tag{2.10}$$

where the independence between $r_h^{(sup)}(k)$ and $r_h^{(s_u)}(k)$, (2.9), (2.5) have been utilized.
The *equivalent* signal to noise ratio (SNR_{eq}) is defined as

$$SNR_{eq} \triangleq \frac{\sigma^2_{r_h^{(s_u)}}}{\sigma_w^2} = \frac{\sigma^2_{s_u}}{\sigma_w^2} = \frac{SNR}{(1+\beta)} \tag{2.11}$$

where (2.9) has been utilized. As stated above, at a given SNR, an increasing of β causes a decreasing of SNR_{eq}.
The sum of $r_h(kT)$ and $w(kT)$ is denoted by $r(kT)$ and the following holds

$$r(kT) = r_h(kT) + w(kT) = r_h^{(s_u)}(kT) + r_h^{(sup)}(kT) + w(kT), \tag{2.12}$$

where (2.8) has been used. The first operation performed at the receiver side is the symbol synchronization. It is accomplished by the peak detection of the signal produced by the filtering of $r(kT)$ by the matching of $p_n^t(kT)$, see def. (2.6). Once synchronized, $r(kT)$ undergoes a rate conversion, which yields the signal $r_{est}(kT_1)$, exploited for channel estimation. The rate conversion of $r_h^{sup}(kT)$ produces a signal that is roughly the cyclic convolution between $p_{sup}(kT_1)$ and the channel $\overline{h}_a(kT_1)$, whose frequency response (FR) is denoted by $\overline{H}_a(f)$ and is related to $H(f)$ in the following way

$$\overline{H}_a(f) = H(f), \quad 0 \leq |f| < \frac{F_1}{2} \tag{2.13}$$

where $F_1 = T_1^{-1}$ and $|\cdot|$ is the absolute value operator. If F_1 is such that the set $\{f : 0 \leq f < F_1\}$ includes the range of frequencies corresponding to the active subcarriers, the estimation of the CFR on the active subcarrier is obtained, as explained in Chapter 5. Namely, if $\mathbf{H}_a$ is a vector whose elements are defined as

$$\mathbf{H}_a[i] \triangleq H(\mathbf{x}_a[i]F_s), \quad i = 1, \ldots N_a \tag{2.14}$$

the estimate $\hat{\mathbf{H}}_a$ of $\mathbf{H}_a$ is obtained. From $\hat{\mathbf{H}}_a$, the impulse response $\hat{h}_a(kT)$ is derived as the truncation to L_h of the result of the following operation

$$\hat{h}_a(kT) = \frac{1}{M} \sum_{i=0}^{N_a-1} \hat{\mathbf{H}}_a[i] e^{-j\frac{2\pi}{M}\mathbf{x}_a[i]k}, \quad k = 0, \ldots, L_h - 1 \tag{2.15}$$

which is the truncated inverse discrete Fourier transform (IDFT) of the signal obtained by filling $\hat{\mathbf{H}}_a$ with zeros at positions corresponding to the virtual carriers, denoted by $\hat{\mathbf{H}}$.

In order to cancel the contribute of $r_h^{(sup)}(kT)$ from $r_h(kT)$, see (2.8), $\hat{h}_a(kT)$ is utilized by the PN-CANC block to compute

$$\hat{r}_h^{(sup)}(kT) = p_n(kT) * \hat{h}_a(KT), \tag{2.16}$$

where $*$ denotes the convolution operator. The signal resulting from the cancelation is denoted by $\hat{r}(kT)$ and is given by

$$\hat{r}(kT) = r_h^{(s_u)}(kT) + p_n(kT) * (\hat{h_a}(kT) - h(kT)) + w(kT) \tag{2.17}$$

The sum of the cancelation error, defined as

$$w_{canc}(kT) \triangleq p_n(kT) * (\hat{h_a}(kT) - h(kT)), \tag{2.18}$$

and the noise $w(kT)$ is denoted by $w_{eq}(kT)$, namely

$$w_{eq}(kT) \triangleq w_{canc}(kT) + w(kT). \tag{2.19}$$

Hence, $\hat{r}(kT)$ can be written as

$$\hat{r}(kT) = r_h^{(s_u)}(kT) + w_{eq}(kT). \tag{2.20}$$

$\hat{r}(kT)$ feeds the demodulation block, which yields M output signals corresponding to the demodulation of each transmitted subcarrier. The vectorial function $\mathbf{u}(nT_0)$ denotes the demodulator output, whose bth component is denoted by $u_b(nT_0)$. Separating the parts related to the demodulation of $r_h^{(s_u)}(kT)$ and $w_{eq}(kT)$, denoted by $\overline{\mathbf{u}}(nT_0)$ and $\overline{\mathbf{w}}(nT_0)$, respectively, $\mathbf{u}(nT_0)$ can be expressed as

$$\mathbf{u}(nT_0) = \overline{\mathbf{u}}(nT_0) + \overline{\mathbf{w}}(nT_0). \tag{2.21}$$

The next block removes values corresponding to the virtual carriers, yielding the signal $\mathbf{u}_a(nT_0)$, whose ith component $u_{a,i}(nT_0)$ corresponds to the active subcarrier $\mathbf{x}_a[i]$, see def. (2.3). Setting $b = \mathbf{x}_a[i]$, $u_{a,i}(nT_0)$ can be expressed as

$$u_{a,i}(nT_0) = \overline{u}_b(nT_0) + \overline{w}_b(nT_0) \tag{2.22}$$

As explained in Chapter 4, under the hypothesis of flat subchannels and static channel during the n'th OFDM symbol, denoted by $\mathbf{H}^{(n')}$, $\overline{u}_b(nT_0)$ is a function of $\mathbf{H}^{(n')}[b']$ and $A_{b'}(n')$ for $b' = b-1, b, b+1$ and $n' = \lfloor n/2 \rfloor - 1, \lfloor n/2 \rfloor, \lfloor n/2 \rfloor + 1$. The equalization is performed as a per branch linear minimum mean square error (LMMSE) equalizers. LMMSE coefficients are computed by the EQ-COEFF block. Theoretically, to compute the exact coefficients, $\mathbf{H}_a$ and $\sigma^2_{\overline{w}}$ are needed, where $\sigma^2_{\overline{w}}$ is the power of $\overline{w}_b$, see (2.21) and (2.22), equal for every branch. In practise, $\hat{\mathbf{H}}_a$ and an estimate of $\sigma^2_{\overline{w}_b}$ are used. The estimation of $\sigma^2_{\overline{w}_b}$ is initialized

to the *system* noise power corresponding to the error free transmission condition. According to this initial value, a first series of equalization coefficients is computed. $\mathbf{u}_a(nT_0)$ is, then, equalized and the subsequent operations of unstaggering, serializing and decoding produce the output bit stream. By re-encoding and re-mapping the output bit stream the estimate, $\hat{\mathbf{A}}_a$, of $\mathbf{A}_a$, see def. (2.4), is obtained. The NOISE ESTIMATION block utilizes $\hat{\mathbf{H}}_a$ and $\hat{\mathbf{A}}$ to compute an estimate, $\hat{\overline{\mathbf{u}}}$, of $\overline{\mathbf{u}}$, and estimates the noise power as, see (2.22),

$$\hat{\sigma^2_{\overline{w}}} = \frac{1}{N_a} \sum_{i=0}^{N_a-1} |u_{\mathbf{x}_a[i]}(nT_0) - \hat{\overline{u}}_{\mathbf{x}_a[i]}(nT_0)|^2 \tag{2.23}$$

This is the value utilized to compute equalization coefficients that will yield the correct output bit stream. The *theoretical* per carrier minimum MSE, denoted by $\mathbf{J}_{min}$, is also computed by the EQ-COEFF block and the information is used to set the initial likelihoods needed for LDPC decoding purposes.

2.2 CD3-OFDM system

Coded decision directed demodulation (CD3) is a channel estimation scheme for coherent demodulation of OFDM presented in [25]. The technique is based on a loop exploiting the error correction capability of the FEC decoder. The OFDM system utilizing the CD3 estimation technique is addressed as CD3-OFDM. In Fig. 2.2, a simplified block diagram of CD3-OFDM system is drawn. Definitions given in the previous section are assumed to be known. To facilitate analogies and comparison between the systems, the same notation has been utilized for main parameters and signals. If needed, superscripts OQAM and CD3 will be used. Encoding, interleaving and QAM constellations are the same as the OFDM/OQAM system. After the virtual carrier insertions, whose number is denoted by N_V, the classical OFDM modulation with cyclic prefix insertion (CP) is perfomed through digital DFT implementation [27]. Namely, the M low rate QAM symbols streams, $\mathbf{A}(n'T_s)$ ($T_s^{CD3} > T_s^{OQAM}$), produced by the S/P block,

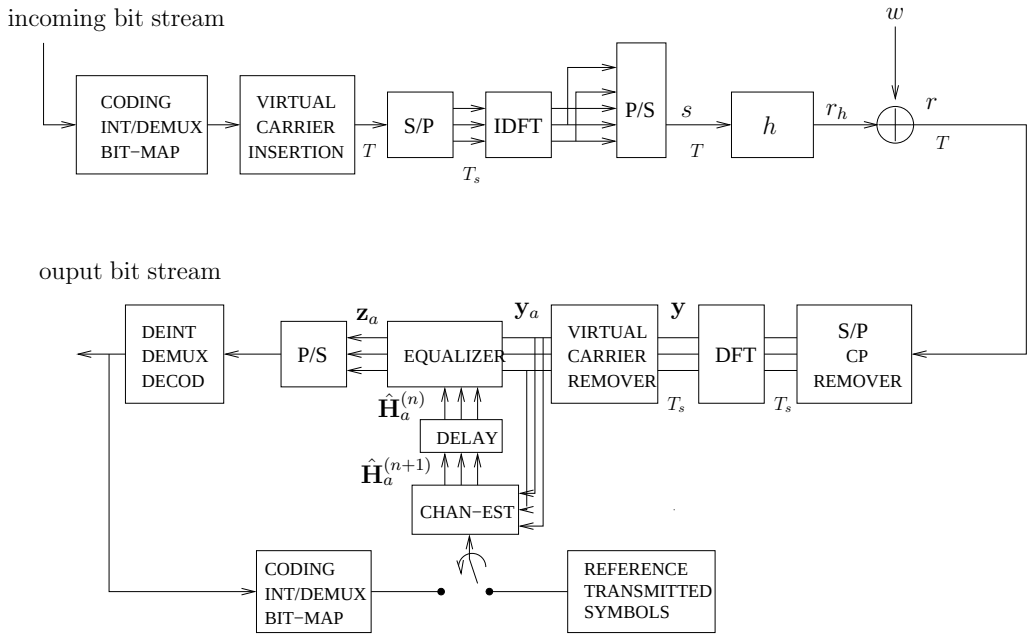

Figure 2.2: High level CD3-OFDM system block diagram.

feed a block which performs the IDFT of the symbols at its input. After the insertion of the CP, namely the replica of a fraction Δ of the IDFT block output, the signal undergoes a S/P conversion, which yields the signal $s(kT)$. CP lenght is denoted by N_{CP} and is equal to $N_{CP} = \Delta M$. The difference between the symbol duration and the time needed to the transmission of the cyclic prefix is denoted by T_u, namely

$$T_u = T_s - N_{CP}T = MT. \tag{2.24}$$

System subcarriers are spaced $F_u = T_u^{-1}$ apart. $s(kT)$ is transmitted through a time variant and frequency selective channel. In the previous section the dependence on the time of the CIR was been implicit. Instead, to explain CD3 receiver, an explicit time reference is needed. Hence, under the hypothesis of a static channel over the time needed to transmit one OFDM symbol, T_s, the CIR is denoted by $h(n'T_s, kT)$. Namely , $h(n'T_s, kT)$ is the CIR value during the transmission of the n'th OFDM symbol. Its Fourier transform is denoted by $H(n', f)$ and its values on active subcarriers are given by $H(n, \mathbf{x}_a[i]F_u),\ i = 0, \ldots, N_a - 1$, where

we recall that $\mathbf{x}_a$ is the ordered set of active indexes (2.3). The notation $\mathbf{H}_a^{(n')}$ is also introduced to denote the vector of CFR values on active subcarriers, namely the ith element of the vector, denoted by $\mathbf{H}_a^{(n)}[i]$, is defined as

$$\mathbf{H}_a^{(n)}[i] \triangleq H(n, \mathbf{x}_a[i]F_u). \tag{2.25}$$

Estimates of $H(n, \mathbf{x}_a[i]F_u)$ and $\mathbf{H}_a^{(n)}$ are denoted by $\hat{H}(n, \mathbf{x}_a[i]F_u)$ and $\hat{H}(n, \mathbf{x}_a[i]F_u)$, respectively.

The filtering of $s(kT)$ by the channel is denoted by $r_h(kT)$. At the receiver side, a circularly symmetric complex Guassian noise, denoted by $w(kT)$, is added. The system SNR is defined as

$$SNR = \frac{\sigma_s^2}{\sigma_w^2} \tag{2.26}$$

where σ_s^2 and σ_w^2 are statistical powers of $s(kT)$ and $w(kT)$, respectively. The signal $r(kT)$, given by the sum of $r_h(kT)$ and $w(kT)$, undergoes a S/P conversion. After the CP removal, the signal is demodulated through the DFT block, yielding the vectorial signal $\mathbf{y}(n'T_s)$, whose bth component corresponds to the branch b and is denoted by $y_b(nT_s)$. The virtual carriers removal block yields the signal denoted by $\mathbf{y}_a(n'T_s)$, whose ith component is defined as follows

$$y_{a,i}(nT_s) = y_{\mathbf{x}_a[i]}(nT_s). \tag{2.27}$$

Denoted by $\mathbf{A}_a(n'T_s)$ the subvector of $\mathbf{A}(n'T_s)$ corresponding to the active indexes and by $\overline{\mathbf{w}}_a(n'T_s)$ the result of noise demodulation on active subcarriers, $\mathbf{y}_a(n'T_s)$ can be expressed as [25]

$$\mathbf{y}_a(n'T_s) = \mathbf{H}_a^{(n')}. * \mathbf{A}_a(n'T_s) + \overline{\mathbf{w}}_a(n'T_s), \tag{2.28}$$

where $.*$ denotes the element wise multiplication. Given the estimate $\hat{\mathbf{H}}_a^{(n')}$, equalization block performs the following operation

$$\mathbf{z}(n'T_s) = \mathbf{y}_a(n'T_s)./\hat{\mathbf{H}}_a^{(n')}, \tag{2.29}$$

where $./$ denotes the element wise division. The CD3 channel estimation works as follows:

- let's denote as n_0T_s an initial reference time, namely the beginning of a basic data unit transmission, e.g. a frame [8];

- a reference sequence, denoted by $\mathbf{R}_a(n_0T_s)$, is transmitted at time n_0T_s;

- the corresponding received signal, after the demodulation and the virtual carrier removal, is given by (2.28)

$$\mathbf{y}_a(n_0T_s) = \mathbf{H}_a^{(n_0)}. * \mathbf{R}_a(n_0T_s) + \overline{\mathbf{w}}_a(n_0T_s). \tag{2.30}$$

- at time n_0T_s is computed the channel estimate that will be used at time $(n_0{+}1)\ T_s$, as the delay element of Fig. 2.2 shows;

- being $\mathbf{R}_a(n_0T_s)$ known at the receiver, the channel estimate is obtained as

$$\hat{\mathbf{H}}_a^{(n_0+1)} = \mathbf{y}_a(n_0T_s)./\mathbf{R}_a(n_0T_s); \tag{2.31}$$

- at time $n'T_s = (n_0 + 1)T_s$, unknown data, $\mathbf{A}_a(n'T_s)$, are sent and the corresponding received signal,

$$\mathbf{y}_a(n'T_s) = \mathbf{H}_a^{(n')}. * \mathbf{A}_a(n'T_s) + \overline{\mathbf{w}}_a(n'T_s), \tag{2.32}$$

  is equalized exploiting the channel estimate derived at the previous time, see (2.31). Namely,

$$\mathbf{z}_a(n'T_s) = \mathbf{y}_a(n'T_s)./\hat{\mathbf{H}}_a^{(n')} \tag{2.33}$$

- from $\mathbf{z}_a(nT_s)$, the output bit stream, $\mathbf{b}^{(n)}$ is obtained by deinterleaving and decoding.

- $\mathbf{b}^{(n')}$ is, then, re-encoded and re-mapped, yielding an estimate of the sent data, $\hat{\mathbf{A}}_a((nT_s)$, whose reliability depends on the error correction power of the code;

- the channel estimate, which will be utilized next, is obtained as

$$\hat{\mathbf{H}}_a^{(n'+1)} = \mathbf{y}_a(n'T_s)./\hat{\mathbf{A}}_a(n'T_s) \tag{2.34}$$

Unlike other OFDM channel estimation techniques [28], CD3-OFDM does not require the transmission of a comb of pilots (transmitted values known at the receiver) tones for channel estimation. Hence, an improvement in spectral efficiency, typically between 5% and 15% is achieved [25]..

Chapter 3

DVB-T2 overview

In this chapter a brief overview of the DVB-T2 standard is given in order to highlight specifications addressed in this work. In particular, after introducing the key DVB standards, the main parameters concerning the DVB-T2 specifications, coding, interleaving and multiplexing will be described in detail.

3.1 Introduction

DVB-T2 is a digital terrestrial transmission system developed by the DVB Project. It is the most advanced such system in the world and introduces the latest modulation and coding techniques to enable highly efficient use of valuable terrestrial spectrum for the delivery of audio, video and data services to fixed, portable and mobile devices. The DVB-T2 specification was approved by the DVB Steering Board at the end of June 2008. On approval it was released as a DVB Blue-Book [8] and sent to ETSI (European Telecommunications Standards Institute) for publication as a formal standard. Vendors are already working on the design of DVB-T2 equipment, with the first prototypes expected by the end of 2008. In parallel, further work will be required within the DVB Project and elsewhere on the creation of implementation guidelines, validation testing, etc.

Towards the end of 1991, broadcasters, equipment manufacturers and regulatory bodies in Europe came together to discuss the formation of a group that

would oversee the introduction of digital TV. That group, which became known as the European Launching Group (ELG), realised that a consensus-based framework, through which all of the key stakeholders could agree on the appropriate technologies to be used, would benefit everybody involved. A Memorandum of Understanding (MoU) was drawn up, setting out the basis on which competitors in the marketplace would come together in a spirit of trust and mutual respect. The MoU was signed in September 1993 by all ELG participants, and the DVB Project was born. A key report from the Working Group on Digital Television was also central to setting out important concepts that would go on to shape the introduction of digital TV in Europe and far beyond.

The first phase of DVB' s work involved establishing standards to enable the delivery of digital TV to the consumer via the "traditional" broadcast networks. Thus, the three key standards during this phase were DVB-S for satellite networks, DVB-C for cable networks and DVB-T for terrestrial networks. In addition to these, a whole range of supporting standards were required covering areas such as service information (DVB-SI), subtitling (DVB-SUB), interfacing (e.g. DVB-ASI), etc... Interactive TV, one of the key advances enabled by the switch from analogue to digital, required the creation of a set of return channel standards and the Multimedia Home Platform (MHP), DVB's open middleware specification. DVB then moved to embrace network convergence through the development of standards using innovative technologies that allow the delivery of DVB services over fixed and wireless telecommunications networks (e.g. DVB-H for mobile TV, DVB-IPTV). The latest phase of DVB's work is a natural progression into areas such as a system for content protection and copy management (DVB-CPCM), and looking at how DVB devices operate in the environment of the home network. DVB is dedicated to constant innovation to keep up with both technological developments and market requirements. Thus we have already seen the scope of DVB-H expanded into the S-band through DVB-SH and, before that, the publication of DVB-S2. 2008 sees the developments of next generation terrestrial (DVB-T2).

DVB-T is the most widely deployed DTT (Digital Terrestrial Television) system worldwide, with services on air in over thirty countries and more than 60 million receivers deployed. Economies of scale have pushed receiver prices downwards constantly, with basic receivers now readily available at a retail price of less than EUR 30.

In the years ahead, in countries where DVB-T services have become well-established, regulators will be keen to achieve full Analogue Switch-Off (ASO), and in the process release valuable UHF and VHF spectrum for other purposes. Some countries have already completed ASO.

One option at ASO will be the introduction of new services using DVB-T2 technology. This could enable, for example, the roll out of new nationwide multiplexes offering multichannel HDTV services, or perhaps innovative new datacasting services.

More than sixty DVB member companies have contributed to the work, which generated hundreds of meeting days and thousands of emails. As with all DVB standards, the final specification is based on a carefully considered set of Commercial Requirements. Key requirements included an increase in capacity and improved robustness. (Current projections suggest that capacity gains of around 45% will be achieved.) The new standard was also required to be able to reuse currently existing receive antennas and downlinks.

DVB-T2 is not designed to replace DVB-T; rather the two standards will coexist in many markets for many years.

3.2 DVB-T2 specifications

As with its predecessor, DVB-T2 uses OFDM (orthogonal frequency division multiplex) modulation, with a large number of sub-carriers delivering a robust signal. Also in common with DVB-T, the new specification offers a range of different modes making it a very flexible standard. In the realm of error correction,

DVB-T2 uses the same coding that was selected for DVB-S2. LDPC (Low Density Parity Check) coding combined with BCH (Bose-Chaudhuri-Hocquengham) coding offers excellent performance in the presence of high noise levels and interference, resulting in a very robust signal. Several options are available in areas such as the number of carriers, guard interval sizes and pilot signals, so that the overheads can be minimised for any target transmission channel. A new technique, called Rotated Constellations, provides significant additional robustness in difficult channels. Also, a mechanism is provided to separately adjust the robustness of each delivered service within a channel to meet the required reception conditions (e.g. in-door antenna/roof-top antenna). This same mechanism allows transmissions to be tailored such that a receiver can save power by decoding only a single programme rather than a whole multiplex of programmes. DVB-T2 also specifies a transmitter diversity method, known as Alamouti coding, which improves coverage in smallscale single-frequency networks. Finally, DVB-T2 has defined a way that the standard can be compatibly enhanced in the future through the use of Future Extension Frames.

In this section the simplified *single input stream* DVB-T2 scheme shown in Fig. 3.1 is addressed in order to get rid of details that are useless for the aim of this work. A bit stream that is the result of preprocessing operations on one or

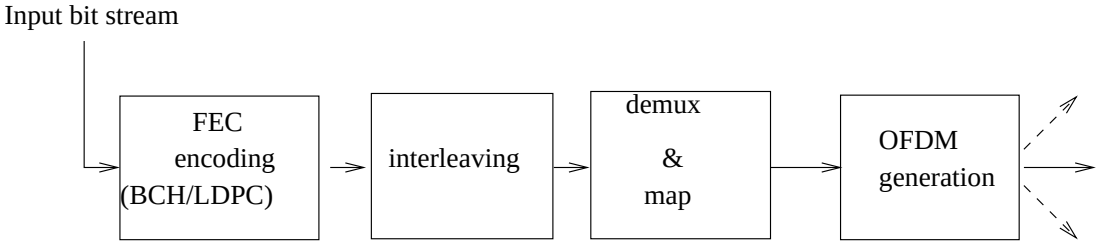

Figure 3.1: Simplified high level DVB-T2 block diagram.

more MPEG-2 Transport Stream(s) and/or one or more Generic Stream(s) is the input of the system.

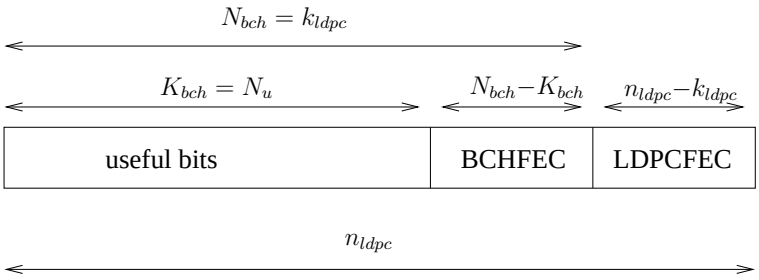

Figure 3.2: LDPC block.

The system output is typically a single signal to be transmitted on a single RF channel (SISO system). Optionally, the system can generate a second set of output signals, to be conveyed to a second set of antennas in what is called MISO transmission mode. The SISO transmission mode is addressed here.

3.3 FEC encoding

A concatenated coding scheme is used both in OQAM and CD3-OFDM systems. Namely, the forward error correction (FEC) encoding consists of a concatenation of t-error correcting BCH outer code and low density parity check (LDPC) inner code, [26]. Fig. 3.2 shows the FEC coded block, whose length has been denoted as n_{ldpc}. BCHFEC and LDPCFEC denote parity bits added after BCH and LDPC processing, respectively. $N_{bch}(n_{ldpc})$, $K_{bch}(k_{ldpc})$ denote the BCH (LDPC) coded and information word lengths, respectively. Only the LDPC block part denoted as *useful bits* will be considered in the spectral efficiency computation as reported in Section 7.1. Its length has been denoted as N_u. The standard provides two LDPC block lengths, namely $n_{ldpc} = 64800$ (normal block) and $n_{ldpc} = 16200$ (short block). Here, the normal block length is considered. The corresponding parameters are reported in Table 3.1. Table 3.2, in particular, highlights the parameters utilized in our simulations. 3.2.

BCH and LDPC details can be found in the DVB-T2 Blue Book [8].

Table 3.1: FEC encoding parameters for normal LDPC block ($n_{ldpc} = 64800$)

$LDPC\,rate$	$K_{bch}(= N_u)$	k_{ldpc}	$BCH\ t-correction$	$N_{bch} - K_{bch}$	n_{ldpc}
1/2	32208	32400	12	192	64800
3/5	38688	38880	12	192	64800
2/3	43040	43200	10	160	64800
3/4	48408	48600	12	192	64800
4/5	51648	51840	12	192	64800
5/6	53840	54000	10	160	64800

Table 3.2: Encoding parameters

$LDPCrate$	$K_{bch}(= N_u)$	k_{ldpc}	$BCHt-correction$	$N_{bch} - K_{bch}$	n_{ldpc}
1/2	32208	32400	12	192	64800

3.4 Interleaving

The output of the LDPC encoder is bit interleaved, namely a parity interleaving followed by a column twist interleaving is performed.

In the parity interleaving part, parity bits are interleaved following the relations

$$u_i = \lambda_i \quad \text{for } 0 \leq \mathrm{i} < \mathrm{k_{ldpc}}\ (\mathrm{informationbitsarenotinterleaved})$$

$$u_{k_{ldpc}+360t+s} = \lambda_{k_{ldpc}+Q_{ldpc}\cdots+t} \quad \text{for } 0 \leq \mathrm{s} < 360,\ 0 \leq \mathrm{t} < \mathrm{Q_{ldpc}}$$

where λ_i are incoming bits, u_i are interleaved bits and Q_{ldpc} is defined by the Table 3.3

According to Table 3.2, in our case $Q_{ldpc} = 25$.

Parameters concerning the *column twist interleaving* configuration for each modulation format and $n_{ldpc} = 64800$ are specified in Table 3.4.

Table 3.3: Q_{ldpc} specification for different coding rates

$LDPC\ Rate$	Q_{ldpc}
1/4	36
1/2	25
3/5	18
2/3	15
3/4	12
4/5	10
5/6	8

Table 3.4: Column twisting interleaving configuration for $n_{ldpc} = 64800$

$Modulation$	$Rows(Nr)$	$Columns(N_c)$
$16QAM$	8100	8
$64QAM$	5400	12
$256QAM$	4050	16

In the column twist interleaving part, the data bits u_i from the parity interleaver are serially written into the column-twist interleaver column-wise, and serially read out row-wise as shown in Figure 3.3, where the write start position of each column is twisted by t_c according to Table 3.5.

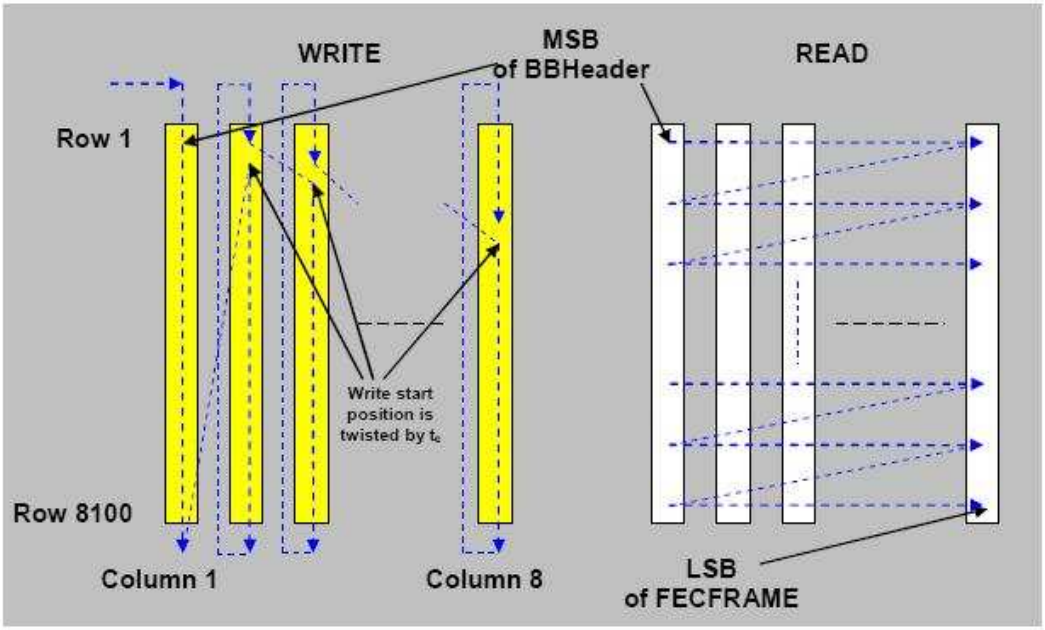

Figure 3.3: Graphical representation of column twist interleaver.

Mathematical formulation of the column twisting interleaving is given in [8].

3.5 Demux & map block

Each FECFRAME, which is the sequence of 64800 bits produced by the encoding and interleaving operations, is mapped to a coded and modulated FEC block by first de-multiplexing the input bits into parallel cell words and then mapping these cell words into constellation values. The number of output data cells and the effective number of bits per cell η_{MOD} is defined by Table 3.6.

Table 3.5: Column twisting interleaving parameters for $n_{ldpc} = 64800$

Mod.	N_c	column twisting parameter t_c															
		$Col.0$	1	2	3	4	5	6	7	8	9	10	11	12	13	14	15
$16QAM$	8	0	0	2	4	4	5	7	7	–	–	–	–	–	–	–	–
$64QAM$	12	0	0	2	2	3	4	4	5	5	7	8	9	–	–	–	–
$256QAM$	16	0	2	2	2	2	3	7	15	16	20	22	22	27	27	28	32

Table 3.6: Parameters for bit mapping into constellation ($\eta_{ldpc} = 64800$)

Modulation mode	η_{MOD}	Number of output data cells
$256QAM$	8	8100
$64QAM$	6	10800
$16QAM$	4	16200

The bit-stream from the bit interleaver v_{d_i} is de-multiplexed into $N_{substreams}$ sub-streams, according to the value given by the Table 3.7.

The de-multiplexing operation is graphically represented in Fig. 3.4.

Table 3.8 gives the correspondence between input bits and stream bits for a $16QAM$ constellation. Similar tables for $64QAM$ and $256QAM$ can be found in [8].

Each cell word produced by the demultiplexer is modulated using either 16-QAM, 64-QAM or 256-QAM constellations to give a point z_q whose exact real

Table 3.7: Sub-streams number for different constellations ($n_{ldpc} = 64800$)

Modulation	$N_{substreams}$
$16QAM$	8
$64QAM$	12
$256QAM$	16

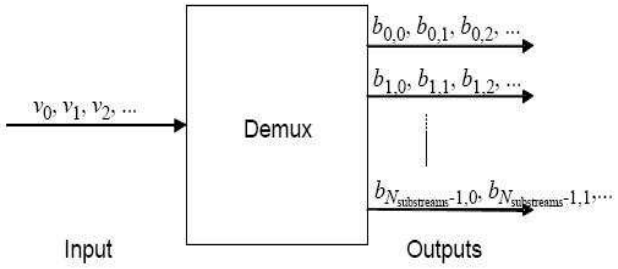

Figure 3.4: Graphical representation of de-multiplexing operation.

Table 3.8: Parameters for de-multiplexing of bits to sub-streams

Modulation format	16QAM							
Input bit−number, d_i mod $N_{substreams}$	0	1	2	3	4	5	6	7
Output bit−number, e	7	1	4	2	5	3	6	0

and imaginary parts are written in the Blue Book. In order to normalize the constellation power, each point z_q is multiplied by a normalization factor. The correct complex cell value f_q is obtained as indicated in Table 3.9.

3.6 OFDM generation

The OFDM generation is a block performing the operations shown in Fig. 3.5. The incoming stream is formed by blocks of N_a active cells which will modulate N_a active subcarriers. The blocks are padded with pilot tones (values known

Table 3.9: Normalization operation

Modulation	Normalization
$16QAM$	$f_q = \frac{z_q}{\sqrt{10}}$
$64QAM$	$f_q = \frac{z_q}{\sqrt{42}}$
$256QAM$	$f_q = \frac{z_q}{\sqrt{170}}$

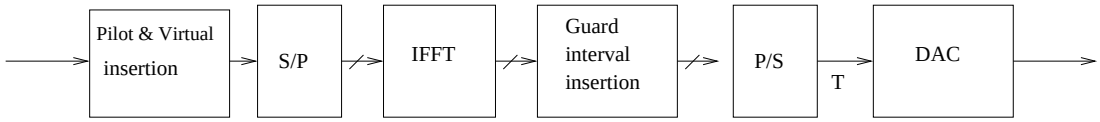

Figure 3.5: OFDM generation

Table 3.10: 8Mhz, 16k extended mode parameters

Total subcarriers ($M = 2N$)	16384
Active subcarriers (N_a)	13921
Cyclic prefix fraction (Δ)	$\frac{1}{8}$
Elementary period (T)	$\frac{7}{64}\,\mu s$
DVB-T channel bandwidth	8 Mhz

at the receiver side exploited for channel estimation purpose) and virtual cells (zeros). The result is a block of M total subcarriers, which undergoes a serial to parallel conversion and an IFFT transform. After duplicating a fraction Δ of the produced block, a parallel to serial conversion in performed. The sampling period T depends on the system clock period and, once the number of active subcarriers have been fixed, its value is constrained by the available bandwidth. Here, 8 Mhz channels are addressed. The Digital to Analog Converter (DAC) yields the baseband equivalent of the transmitted signal. A translation to a nominal center frequencies f_c belonging to VHF and UHF band is performed to obtain the transmitted signal. Parameters regarding the 8Mhz, 16k extended mode are specified In Table 3.10.

3.7 Spectrum constraints

Spectrum masks for cases where a transmitter for digital terrestrial television is co-sited with, and operating on a channel adjacent to, a transmitter for analogue television are given in Fig. 3.6 and Table 3.11 for the following analogue television systems [3]:

- G/PAL/A2 and G/PAL/NICAM;

- I/PAL/NICAM;

- K/SECAM and K/PAL;

- L/SECAM/NICAM.

The masks shown in Fig. 3.6 cover the minimum protection needed for analogue television.

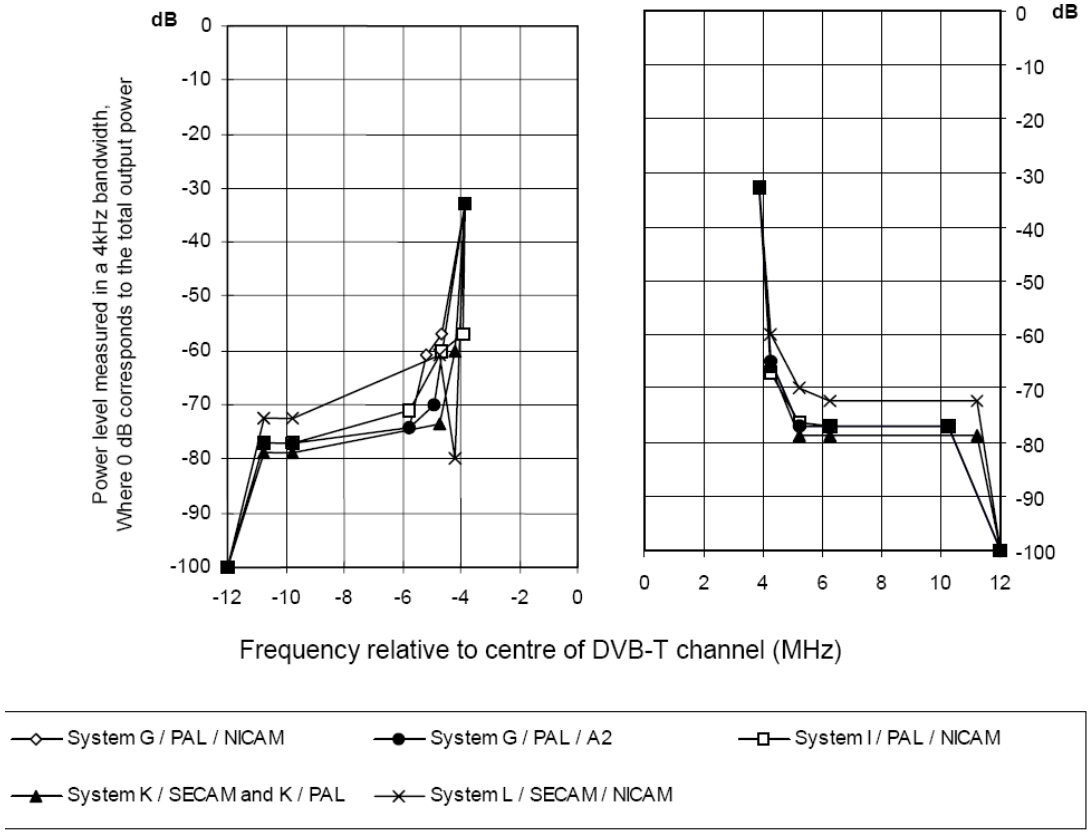

Figure 3.6: Spectrum masks for a digital terrestrial television transmitter operating on a lower or higher adjacent channel to a co-sited analogue television transmitter

Table 3.11: Breakpoints for spectrum mask

Breakpoints									
G/PAL / NICAM		G/PAL / A2		I/PAL / NICAM		K/SECAM K/PAL		L/SECAM / NICAM	
rel. freq. MHz	rel. level dB	rel. freq. MHz	rel. level dB	rel. freq. MHz	rel. level dB	rel. freq. MHz	rel. level dB	rel. freq. MHz	rel. level dB
-12	-100	-12	-100	-12	-100	-12	-100	-12	-100
-10,75	-76,9	-10,75	-76,9	-10,75	-76,9	-10,75	-78,7	-10,75	-72,4
-9,75	-76,9	-9,75	-76,9	-9,75	-76,9	-9,75	-78,7	-9,75	-72,4
-5,75	-74,2	-5,75	-74,2	-5,75	-70,9	-4,75	-73,6	-4,75	-60,9
-5,185	-60,9	-5,185	n.a.	-4,685	-59,9	-4,185	-59,9	-4,185	-79,9
n.a.	n.a.	-4,94	-69,9	n.a.	n.a.	n.a.	n.a.	n.a.	n.a.
-4,65	-56,9	n.a.	n.a.	-3,925	-56,9	n.a.	n.a.	-4,65	n.a.
-3,9	-32,8	-3,9	-32,8	-3,9	-32,8	-3,9	-32,8	-3,9	-32,8
+3,9	-32,8	+3,9	-32,8	+3,9	-32,8	+3,9	-32,8	+3,9	-32,8
+4,25	-64,9	+4,25	-64,9	+4,25	-66,9	+4,25	-66,1	+4,25	-59,9
+5,25	-76,9	+5,25	-76,9	+5,25	-76,2	+5,25	-78,7	+5,25	-69,9
+6,25	-76,9	+6,25	-76,9	+6,25	-76,9	+6,25	-78,7	+6,25	-72,4
+10,25	-76,9	+10,25	-76,9	+10,25	-76,9	+11,25	-78,7	+11,25	-72,4
+12	-100	+12	-100	+12	-100	+12	-100	+12	-100

3.8 Channel Model

The performance of the system has been simulated with the channel model for fixed reception F_1 [3]. The Ricean fading channel (F1) defined in the DVB-T specification ETSI EN 300 744 is used to describe the fixed outdoor rooftop antenna reception conditions. The channel does not include any Doppler and should therefore be considered as a snapshot of a real time variant channel. The model has 21-taps. The model is defined by:

$$y(t) = \frac{\rho_0 x(t) + \sum_{i=1}^{N} \rho_i e^{-j\theta_i} x(t-\tau_i)}{\sqrt{\sum_{i=0}^{N} \rho_i^2}} \tag{3.1}$$

where

- the first term before the sum represents the line of sight ray;
- N is the number of echoes equals to 20;
- θ_i is the phase shift from scattering of the ith path - listed in Table 1;
- ρ_i is the attenuation of the ith path - listed in Table 3.12;
- τ_i is the relative delay of the ith path - listed in Table 3.12.

The Ricean factor K (the ratio of the power of the direct path (the line of sight ray) to the reflected paths) is given as

$$K = \frac{\rho_0^2}{\sum_{i=1}^{N} \rho_i^2}. \tag{3.2}$$

Here, the Ricean factor $K = 10$ dB has been used. Hence

$$\rho_0 = \sqrt{10 \sum_{i=1}^{N} \rho_i^2}. \tag{3.3}$$

Table 3.12: Relative power, phase and delay values for chF_1

i	ρ_i	τ_i [µs]	θ_i [rad]
1	0,057 662	1,003 019	4,855 121
2	0,176 809	5,422 091	3,419 109
3	0,407 163	0,518 650	5,864 470
4	0,303 585	2,751 772	2,215 894
5	0,258 782	0,602 895	3,758 058
6	0,061 831	1,016 585	5,430 202
7	0,150 340	0,143 556	3,952 093
8	0,051 534	0,153 832	1,093 586
9	0,185 074	3,324 866	5,775 198
10	0,400 967	1,935 570	0,154 459
11	0,295 723	0,429 948	5,928 383
12	0,350 825	3,228 872	3,053 023
13	0,262 909	0,848 831	0,628 578
14	0,225 894	0,073 883	2,128 544
15	0,170 996	0,203 952	1,099 463
16	0,149 723	0,194 207	3,462 951
17	0,240 140	0,924 450	3,664 773
18	0,116 587	1,381 320	2,833 799
19	0,221 155	0,640 512	3,334 290
20	0,259 730	1,368 671	0,393 889

Chapter 4

OFDM/OQAM: interference analysis and active subcarriers computation

In this chapter a brief overview of the discrete baseband equivalent of the OFDM/OQAM transceiver is given. In order to support and facilitate interference analysis, functions $A(\delta n, \delta b)$ and $G(\delta n, \delta b)$, see def. (4.17) and (4.18), are introduced and their values are computed for the discrete truncated $\mathfrak{I}(t)$ function. Due to the digital implementation of the transceiver, $A(\delta n, \delta b)$ turns out to be a useful *discrete alternative* to the ambiguity function [29].
The number of active subcarriers yielding a transmitted signal with a spectrum satisfying mask constraints described in Chapter 3 is also computed.

4.1 OFDM/OQAM tranceiver

In Fig. 4.1, three blocks of the scheme shown in Fig. 2.1 are reported. Operations performed by the blocks are better explained in the following, in order to clearly introduce all the specifications needed to completely define the transceiver. The OFDM/OQAM modulator is denoted by OQAM MOD and is enclosed by a thicker box. In Fig. 4.2 other three blocks of Fig. 2.1 are reported. All three

blocks belong to the receiver, but only the OFDM/OQAM demodulator, denoted by OQAM DEMOD, will be addressed in this section. The following hypothesis

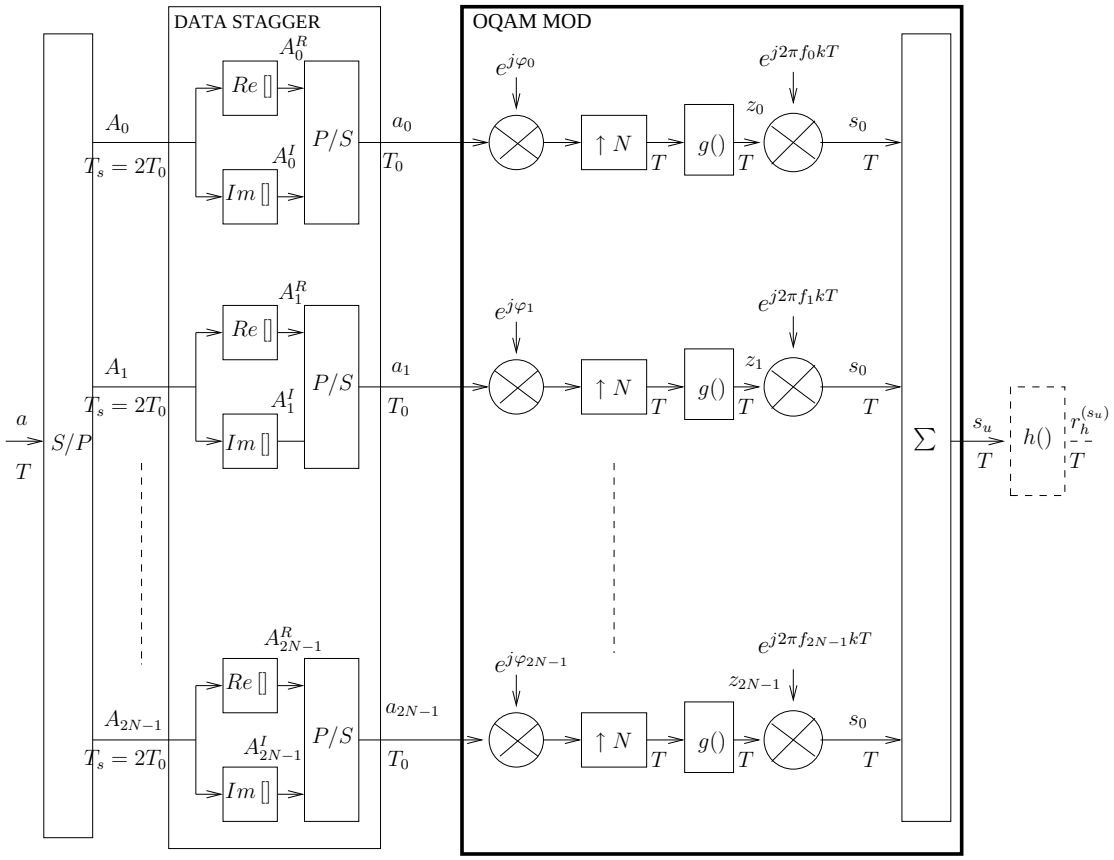

Figure 4.1: OFDM/OQAM modulator.

and definitions hold:

- N is defined as half of the system subcarriers, M;

- $a(kT)$ are incoming symbols drawn from a QAM constellation;

- S/P conversion produces $2N$ low rate QAM streams, denoted by $A_b(n'T_s)$, $b = 0, \ldots, 2N-1$. The real and imaginary part of $A_b(n'T_s)$ are denoted by $A_b^R(n'T_s)$ and $A_b^I(n'T_s)$, respectively. For any b, $b \in [0, \ldots, 2N-1]$, $A_b(n'T_s)$ is modeled as a zero mean stationary stochastic process with independent

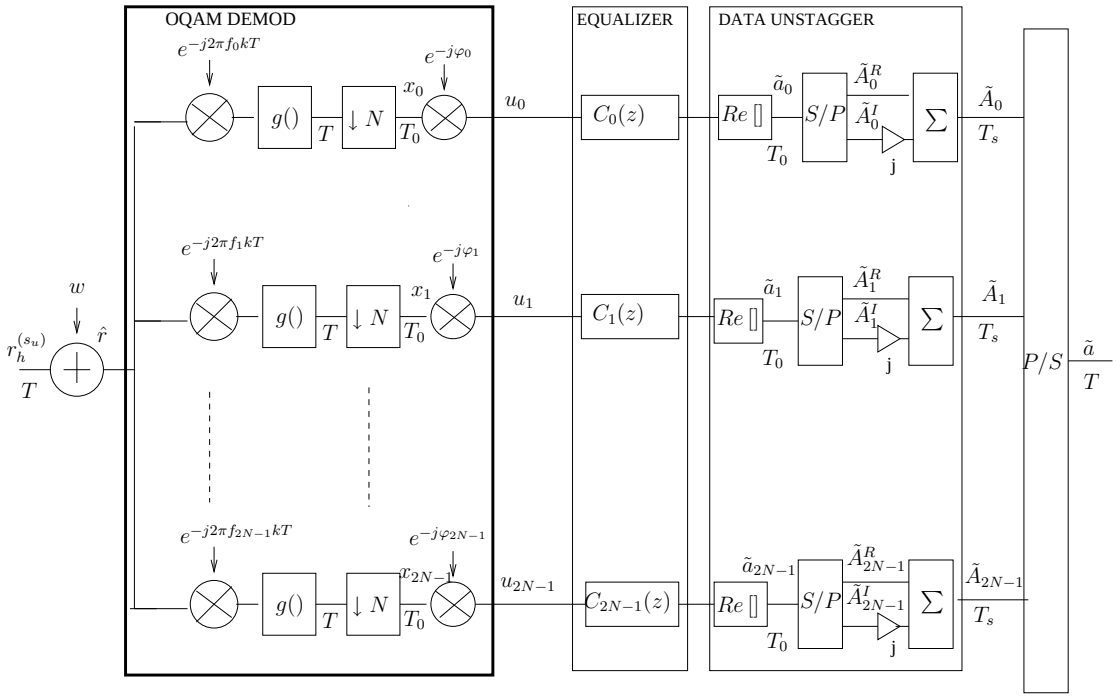

Figure 4.2: OFDM/OQAM receiver with per branch linear equalizers.

identically distributed (i.i.d.) samples. Moreover, real and imaginary parts are assumed to be independent and with equal power. Given any two stationary random processes $x(n'T_s)$ and $y(n'T_s)$, we denote by $r_x(\nu'T_s)$ and $r_{x,y}(\nu'T_s)$ the autocorrelation and crosscorrelation between $x(n'T_s)$ and $y(n'T_s)$, respectively. Hence, for any b the following hold

$$r_{A_b}(\nu'T_s) \triangleq \mathrm{E}\left[A_b(n'T_s)A_b^*((n'-\nu')T_s)\right] = \begin{cases} 0 & \text{for} \nu' \neq 0 \\ \sigma_A^2 & \text{for } \nu' = 0 \end{cases} \tag{4.1}$$

$$r_{A_b^R}(\nu'T_s) \triangleq \mathrm{E}\left[A_b^R(n'T_s)A_b^R((n'-\nu')T_s)\right] = \begin{cases} 0 & \text{for } \nu' \neq 0 \\ \frac{\sigma_A^2}{2} & \text{for } \nu' = 0 \end{cases} \tag{4.2}$$

$$r_{A_b^I}(\nu'T_s) \triangleq \mathrm{E}\left[A_b^I(n'T_s)A_b^I((n'-\nu')T_s)\right] = \begin{cases} 0 & \text{for} \nu' \neq 0 \\ \frac{\sigma_A^2}{2} & \text{for } \nu' = 0 \end{cases} \tag{4.3}$$

Moreover, independence between different branches is assumed. Hence, the following hold for any couple of branches b_1, b_2, with $b_1 \neq b_2$

$$r_{A_{b_1},A_{b_2}}(\nu' T_s) \triangleq \mathrm{E}\left[A_{b_1}(n'T_s)A^*_{b_2}((n'-\nu)T_s)\right] = 0 \quad \forall \nu' \tag{4.4}$$

$$r_{A^R_{b_1}A^R_{b_2}}(\nu' T_s) \triangleq \mathrm{E}\left[A^R_{b_1}(n'T_s)A^R_{b_2}((n'-\nu)T_s)\right] = 0 \quad \forall \nu' \tag{4.5}$$

$$r_{A^I_{b_1},A^I_{b_2}}(\nu') \triangleq \mathrm{E}\left[A^I_{b_1}(n'T_s)A^I_{b_2}((n'-\nu')T_s)\right] = 0 \quad \forall \nu' \tag{4.6}$$

$$r_{A^R_{b_1},A^I_{b_2}}(\nu' T_s) \triangleq \mathrm{E}\left[A^R_{b'}(n'T_s)A^I_{b'}((n'-\nu')T_s)\right] = 0 \quad \forall \nu' \tag{4.7}$$

$$r_{A^I_{b_1},A^R_{b_2}}(\nu' T_s) = r_{A^R_{b_1},A^I_{b_2}}(\nu' T_s) \quad \forall \nu' \tag{4.8}$$

- $Re[\cdot]$ and $Im[\cdot]$ denote the real and imaginary part operators. The DATA STAGGERING block produces $2N$ real streams, $a_b(nT_0)$, $b = 0, \ldots, 2N-1$, by taking, first, the real and imaginary part of incoming streams and, then, serializing them. Namely for $b = 0, \ldots, 2N-1$,

$$\begin{aligned} a_b(2nT_0) &= A^R_b(nT_s) \\ a_b((2n+1)T_0) &= A^I_b(nT_s). \end{aligned} \tag{4.9}$$

From (4.1)–(4.8), for $b = 0 \ldots, 2N-1$

$$r_{a_b}(\nu T_s) \triangleq \mathrm{E}\left[a_b(nT_0)a_b((n-\nu)T_0)\right] = \begin{cases} 0 & \text{for } \nu \neq 0 \\ \frac{\sigma^2_A}{2} & \text{for } \nu = 0 \end{cases} \tag{4.10}$$

and for any couple of branches b_1, b_2, with $b_1 \neq b_2$

$$r_{a_{b_1},a_{b_2}}(\nu) \triangleq \mathrm{E}\left[a_{b_1}(nT_s)a_{b_2}((n-\nu)T_s)\right] = 0 \quad \forall \nu. \tag{4.11}$$

- $a_b(nT_0)$, $b = 0, \ldots, 2N-1$, feed the OFDM/OQAM modulator. For any b, $b = 0, \ldots, M-1$, $\varphi_b(nT_0)$, is defined as follows

$$\varphi_b(nT_0) = \frac{\pi}{2}(b+n) - \pi bn \tag{4.12}$$

  according to the efficient modulator/demodulator implementation proposed in [14]. The first operation of the modulator is to multiply each incoming real stream $a_b(nT_0)$ by $e^{j\varphi_b(nT_0)}$.

- $\uparrow N$ denotes the interpolation operation. As showed in Fig. 4.1, $a_b(nT_0)$, $b = 0, \ldots, 2N-1$, are interpolated and, then, filtered by $g(kT)$, yielding the signals $z_b(nT)$, $b = 0, \ldots, 2N-1$;

- $g(kT)$ is called prototype filter. It is obtained by scaling, sampling and truncating the continuous time $\mathfrak{I}(t)$ function, namely the prototype function of the IOTA transform, [16]. $\mathfrak{I}(t)$ is shown in Fig. 4.3 in linear and logarithmic scale, where $\tau = 1/\sqrt{2}$. $\mathfrak{I}(t)$ is an eigenfunction of the Fourier transform, namely its Fourier transform is equal to itself. Hence, Fig. 4.3 can be interpreted as the graphic of the $\mathfrak{I}(t)$ Fourier transform by substituting t with f on x axis. $g(kT)$ is defined as

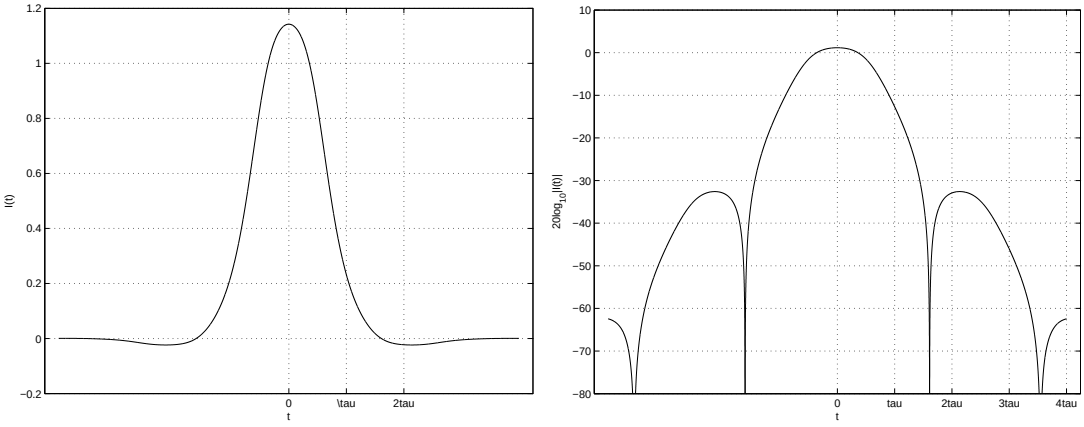

(a) Linear scale (b) Logarithmic scale

Figure 4.3: $\mathfrak{I}(t)$ in linear and logarithmic scale.

$$g(kT) \triangleq \sqrt{\frac{\tau}{N}}\mathfrak{I}\left(k\frac{\tau}{N}\right), \quad k = -\frac{L}{2}, \ldots, \frac{L}{2} - 1, \tag{4.13}$$

where L is the prototype filter length. We define $g_{b,n}(kT)$, $b = 0, \ldots, 2N$, as

$$g_{b,n}(kT) \triangleq j^{b+n} e^{j2\pi b \frac{1}{2\tau} k \frac{\tau}{N}} g((k - nN)T) \tag{4.14}$$

where j is the imaginary unit. If $g(kT)$ has an infinite length, the following holds

$$Re\left[\sum_{k=-\infty}^{+\infty} g_{b_1,n_1}(kT) g'_{b_2,n_2}(kT)\right] = \begin{cases} 1 & \text{for } (\mathrm{b}_1, \mathrm{n}_1) = (\mathrm{b}_2, \mathrm{n}_2) \\ 0 & \text{for } (\mathrm{b}_1, \mathrm{n}_1) \neq (\mathrm{b}_2, \mathrm{n}_2) \end{cases} \tag{4.15}$$

where $'$ denotes the transpose conjugate operator, [14], [16]. Conditions (4.15) are called orthogonality conditions. Thanks to the time localization of $\mathfrak{I}(t)$, if L is large enough, (4.15) are almost satisfied. Here, $L = 4M$ is the value chosen for the filter length.

We, now, rewrite $\sum_{k=-\infty}^{+\infty} g_{b_1,n_1}(kT) g'_{b_2,n_2}(kT)$ in order to introduce the function $A(\delta n, \delta b)$. Namely, from the definition (4.14) follows

$$\begin{aligned}
&\sum_{k'=-\infty}^{+\infty} g_{b_1,n_1}(k'T) g'_{b_2,n_2}(k'T) \\
&= j^{b1-b2} j^{n1-n2} \sum_{k'=-\infty}^{+\infty} e^{j2\pi(f_{b_1} - f_{b_2} k'T)} g((k' - n_1 N)T) g((k' - n_2 N)T) \\
&= j^{b1-b2} j^{n1-n2} (-1)^{(b1-b2)n_1} \sum_{k=-\infty}^{+\infty} e^{j\frac{2\pi}{2N}(b_1 - b_2)k} g(kT) g((k + (n_1 - n_2)N)T)
\end{aligned} \tag{4.16}$$

where (4.23) and the variable change $k = k' - n_1 N$ have been utilized. If N is even, the function $A(\delta n, \delta b)$ is defined as

$$\begin{aligned}
A(\delta n, \delta b) \quad &\triangleq \quad \sum_{k'=-\infty}^{+\infty} g((k' - \delta n \frac{N}{2})T) g((k' + \delta n \frac{N}{2})T) e^{-j\frac{2\pi}{2NT}(-\delta b)k'T} \\
&\overset{(k=k'-\delta n\frac{N}{2})}{=} \quad j^{\delta b \delta n} \sum_{k=-\infty}^{+\infty} e^{j\frac{2\pi}{2N}\delta b k} g(kT) g((k + \delta n N)T).
\end{aligned} \tag{4.17}$$

Being $g(kT)$ even, it implies that $g((k-\delta n\frac{N}{2})T)g((k+\delta n\frac{N}{2})T)$ is also even. Hence, $A(\delta n, \delta b)$ is real, being the Fourier transform of $g(k-\delta n\frac{N}{2})g(k+\delta n\frac{N}{2})$ computed in $\frac{-\delta b}{2NT}$. From (4.15) and (4.16), by defining $G(\delta n, \delta b)$ as

$$G(\delta n, \delta b) \triangleq j^{\delta b} j^{\delta n} j^{-\delta b \delta n} A(\delta n, \delta b), \tag{4.18}$$

the following holds

$$\begin{aligned} Re\left[G(\delta n, \delta b)\right] &= Re\left[(-1)^{\delta b \delta n} j^{\delta b} j^{\delta n} j^{-\delta b \delta n} A(\delta n, \delta b)\right] \\ &= (-1)^{\delta b\, n}(-1)^{\delta b \delta n} Re\left[\sum_{k=-\infty}^{+\infty} g_{\delta b+b,n}(kT) g'_{b,n-\delta n}(kT)\right] \\ &= \begin{cases} 1 & (\delta n, \delta b) = (0,0) \\ 0 & (\delta n, \delta b) \neq (0,0) \end{cases} . \end{aligned} \tag{4.19}$$

Hence,

$$A(\delta n, \delta b) = 0 \quad \text{for } \delta b, \delta n \text{ even, } (\delta \mathrm{b}, \delta \mathrm{n}) \neq (0,0) \tag{4.20}$$

$$G(\delta n, \delta b) = \begin{cases} 0 & \delta b, \delta n \text{ even, } (\delta \mathrm{b}, \delta \mathrm{n}) \neq (0,0) \\ \text{purely imaginary} & (\delta b, \delta n) \neq (0,0) \mod 2 \end{cases} \tag{4.21}$$

where mod is the module operator, namely $a \mod b = a - \lfloor \frac{a}{b} \rfloor b$. Note that N even implies that M is divisible by 4. Hence

$$\begin{aligned} G(\delta n, \delta b + M) &= j^{\delta b + 4(\frac{M}{4})} j^{\delta n} j^{-(\delta b + 4(\frac{M}{4}))\delta n} A(\delta n, \delta b + M) \\ &= j^{\delta b} j^{\delta n} j^{-\delta b \delta n} A(\delta n, \delta b) \\ &= G(\delta n, \delta b) \end{aligned} \tag{4.22}$$

In Table 4.1 and 4.2, values of $A(\delta n, \delta b)$ and $G(\delta n, \delta b)$ are reported for $L = 4M$. Values less than 10^{-3} have been approximated to 0;

- for any b, $b = 0, \ldots, 2N-1$, f_b is defined as

$$f_b \triangleq \frac{1}{MT} \tag{4.23}$$

and represents the carrier spacing. The modulated signal $s_u(kT)$ is obtained by summing all signals produced by multiplying $z_b(nT)$ by $e^{j2\pi f_b kT}$, $b = 0, \ldots, 2N-1$;

Table 4.1: $A(\delta n, \delta b)$ for $L = 4M$

δn / δb	-4	-3	-2	-1	0	1	2	3	4
-4	0	0	0	0.002	0	0.002	0	0	0
-3	0	0	-0.002	0.01	-0.018	0.01	-0.002	0	0
-2	0	-0.002	0	0.038	0	0.038	0	-0.002	0
-1	0.001	0.01	0.038	0.228	0.441	0.228	0.038	0.01	0.001
0	0	-0.018	0	0.441	1	0.441	0	-0.018	0
1	0.001	0.01	0.038	0.228	0.441	0.228	0.038	0.01	0.001
2	0	-0.002	0	0.038	0	0.038	0	-0.002	0
3	0	0	-0.002	0.01	-0.018	0.01	-0.002	0	0
4	0	0	0	0.002	0	0.002	0	0	0

Table 4.2: $G(\delta n, \delta b)$ for $L = 4M$

δn / δb	-4	-3	-2	-1	0	1	2	3	4
-4	0	0	0	-j0.002	0	j0.002	0	0	0
-3	0	0	-j0.002	j0.01	-j0.018	j0.01	-j0.002	0	0
-2	0	-j0.002	0	-j0.038	0	j0.038	0	j0.002	0
-1	-j0.001	j0.01	-j0.038	+j0.228	-j0.441	j0.228	-j0.038	j0.01	-j0.001
0	0	-j0.018	0	-j0.441	1	j0.441	0	j0.018	0
1	j0.001	j0.01	j0.038	j0.228	j0.441	j0.228	j0.038	j0.01	j0.001
2	0	-j0.002	0	-j0.038	0	j0.038	0	j0.002	0
3	0	0	j0.002	j0.01	j0.018	j0.01	j0.002	0	0
4	0	0	0	-j0.002	0	j0.002	0	0	0

- the received signal, denoted by $r_h^{(s_u)}(kT)$, is the result of the filtering of $s_u(kT)$ by the channel $h(kT)$.

- before demodulating $r_h^{(s_u)}(kT)$, the noise $w_{eq}(kT)$ is added, yielding the signal

$$\hat{r}(kT) \triangleq r_h^{(s_u)}(kT) + w_{eq}(kT). \tag{4.24}$$

$w_{eq}(kT)$ is modeled as a zero mean random process with i.i.d. complex circularly symmetric gaussian samples with $\mathrm{E}[|w_{eq}(kT)|^2] = \sigma^2_{w_{eq}}$. Hence,

$$r_{w_{eq}}(\tau T) \triangleq \mathrm{E}\left[w_{eq}(kT)w'_{eq}((k-\tau)T)\right] = \begin{cases} 0 & \text{for } \tau \neq 0 \\ \frac{\sigma^2_{w_{eq}}}{2} & \text{for } \tau = 0 \end{cases} \tag{4.25}$$

$$r_{w^R_{eq}}(\tau T) \triangleq \mathrm{E}\left[w^R_{eq}(kT)w^R_{eq}((k-\tau)T)\right] = \begin{cases} 0 & \text{for } \tau \neq 0 \\ \frac{\sigma^2_{w_{eq}}}{2} & \text{for } \tau = 0 \end{cases} \tag{4.26}$$

$$r_{w^I_{eq}}(\tau T) \triangleq \mathrm{E}\left[w^I_{eq}(kT)w^I_{eq}((k-\tau)T)\right] = \begin{cases} 0 & \text{for } \tau \neq 0 \\ \frac{\sigma^2_{w_{eq}}}{2} & \text{for } \tau = 0 \end{cases} \tag{4.27}$$

$$r_{w^R_{eq},w^I_{eq}}(\tau T) \triangleq \mathrm{E}\left[w^R_{eq}(kT)w^I_{eq}((k-\tau)T)\right] = 0 \quad \forall\tau \tag{4.28}$$

$$r_{w^I_{eq},w^R_{eq}}(\tau T) = r_{w^R_{eq},w^I_{eq}}(\tau T) \quad \forall\tau. \tag{4.29}$$

Note that the cancelation operation shown in Fig. 2.1, is not shown in Fig. 4.2. The effect of the cancelation is taken into account summing the equivalent noise, $w_{eq}(kT)$, defined in (2.19) as $w_{eq}(kT) = w_{canc}(kT)+w(kT)$. If a perfect cancelation is assumed, $w_{eq}(kT) = w(kT)$, where $w(kT)$ is the system noise defined in Chapter 2;

- $\hat{r}(kT)$ is the input of the OFDM/OQAM demodulator. As shown in Fig. 4.2, the demodulator input is split in $2N$ branches. Each branch b performs a multiplication by $e^{-j2\pi f_b T}$ and a filtering by $g(kT)$, see def. (4.13), yielding the signal $x_b(kT)$, $b = 0 \dots 2N-1$. The bth output of the demodulator $u_b(nT_0)$, $b = 0 \dots 2N-1$ is, then, given by the sampling of $x_b(kT)$, namely

$$u_b(nT_0) = x_b(nNT). \tag{4.30}$$

  In Fig. 4.2 sampling operation is denoted by $\downarrow N$.

4.1.1 Signal analysis

In this section relations between $u_b(nT_0)$, $b = 0, \dots, 2N-1$, and $a_{b'}(kT)$, $b' = 0, \dots, 2N-1$, are derived.

We rewrite eq. (2.22), by replacing the subscript i with the corresponding branch $b = \mathbf{x}_a[i]$,

$$u_b(nT_0) = \overline{u}_b(nT_0) + \overline{w}_b(nT_0), \quad b = 0, \dots, 2N-1. \tag{4.31}$$

where $\overline{u}_b(nT_0)$ and $\overline{w}_b(nT_0)$ are the signals resulting by the demodulation of $r_h^{(s_u)}(kT)$ and $w_{eq}(kT)$, respectively. $\overline{u}_b(nT_0)$, $b = 0, \dots, 2N-1$, can be expressed as

$$\overline{u}_b(nT_0) = \sum_{b'=0}^{2N-1} u_{b'b}(nT_0) \tag{4.32}$$

where $u_{b'b}(nT_0)$ is the contribute to $\overline{u}_b(nT_0)$ given by the input branch b'. Fig. 4.4 represents the relation between the b'th input of the modulator, $a_{b'}(nT)$, and the bth output of the demodulator $u_{b'b}(nT_0)$. The scheme is equivalent to the one

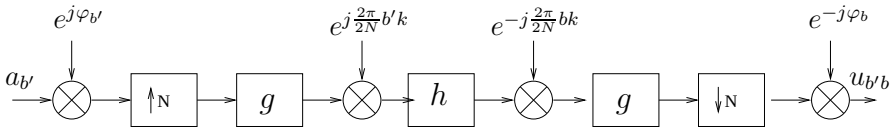

Figure 4.4: Block diagram representing the relation between $a_b(nT_0)$ and $u_{b'b}(nT_0)$

reported in Fig. 4.5. As indicated in the figure, we define $v(kT)$ as

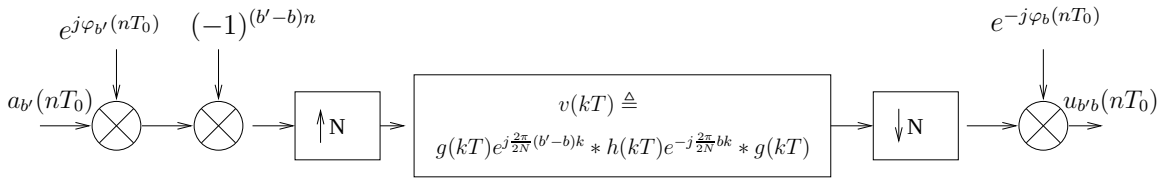

Figure 4.5: Equivalent scheme representing the relation between $a_b(nT_0)$ and $u_{b'b}(nT_0)$.

$$\begin{aligned} v(kT) &\triangleq g(kT)e^{j\frac{2\pi}{2N}(b'-b)k} * h(kT)e^{-j\frac{2\pi}{2N}bk} * g(kT) \\ &= \sum_{k_1=-\infty}^{\infty} g(k_1T)e^{j\frac{2\pi}{2N}(b'-b)k_1} \sum_{k_2=0}^{L_h} h(k_2T)e^{-j\frac{2\pi}{2N}bk_2} g((k_1-k+k_2)T) \end{aligned} \tag{4.33}$$

where the symmetry of $g(kT)$ has been utilized. If the channel length is smaller enough with respect to $2N$ (we recall that in our case $2N = 16384$), the following holds

$$g((k_1-k+k_2)T) \cong g((k_1-k)T), \quad \text{for } \mathrm{k_2} = 0, \ldots, \mathrm{L_h} - 1 \tag{4.34}$$

where $\cong$ means almost equal. Hypothesis (4.34) implies flat subchannel condition. Indeed, (4.33) becomes

$$v(kT) = \mathbf{H}[b] \sum_{k_1=-\infty}^{\infty} g(k_1T)e^{j\frac{2\pi}{2N}(b'-b)k_1} g((k_1-k)T) \tag{4.35}$$

where, we recall from (2.7) that

$$\mathbf{H}[b] \triangleq H\left(b\frac{1}{MT}\right) = \sum_{k=0}^{L_h} h(kT)e^{-j\frac{2\pi}{2N}bk} \tag{4.36}$$

is the DFT of the CIR $h(kT)$ over $2N$ samples. As shown in Fig. 4.5, $u_{b'b}(nT_0)$ can be written as

$$\begin{aligned} u_{b'b}(nT_0) &= e^{-j\varphi_b(nT_0)} \sum_{n_1=-\infty}^{+\infty} a_{b'}(n_1T_0)e^{j\varphi_{b'}(n_1T_0)}v((nN-n_1N)T) \\ &= \mathbf{H}[b]e^{-j\varphi_b(nT_0)} \sum_{n_1=-\infty}^{+\infty} a_{b'}(n_1T_0)e^{j\varphi_{b'}(n_1T_0)} \\ &\quad \sum_{k=-\infty}^{\infty} g(kT)e^{j\frac{2\pi}{2N}(b'-b)k}g((k+(n1-n)N)T) \\ &\overset{(\delta n=n_1-n)}{=} \mathbf{H}[b] \\ &\quad \sum_{\delta n=-\infty}^{+\infty} a_{b'}((\delta n+n)T_0)e^{j\varphi_{b'}((n+\delta n)T_0)}e^{-j\varphi_b(nT_0)}A(\delta n, b'-b) \end{aligned} \tag{4.37}$$

where the definition (4.17) has been utilized. From definition (4.12) follows

$$\begin{aligned} e^{j\varphi_{b'}((\delta n+n)T_0)}e^{-j\varphi_b(nT_0)} &= e^{j(\frac{\pi}{2}(b'+\delta n+n)-\pi b'(\delta n+n)-\frac{\pi}{2}(b+n)+\pi bn)} \\ &= j^{b'-b}j^{\delta n}(-1)^{(b'-b)n}(-1)^{b'\delta n}. \end{aligned} \tag{4.38}$$

Hence, by setting $\delta b = b' - b$, (4.38) becomes

$$\begin{aligned} u_{b'b}(nT_0) &= \mathbf{H}[b] \\ &\quad \sum_{\delta n=-\infty}^{+\infty} a_{b+\delta b}((n+\delta n)T_0)(-1)^{b\delta n}j^{\delta b}j^{\delta n}j^{-\delta b\delta n}A(\delta n, \delta b) \\ &= \mathbf{H}[b] \sum_{\delta n=-\infty}^{+\infty} a_{b+\delta b}((n+\delta n)T_0)(-1)^{b\delta n}G(\delta n, \delta b) \end{aligned} \tag{4.39}$$

where the definition (4.18) has been utilized. From (4.32), for $b = 0, \ldots, 2N-1$,

$$\begin{aligned}
\overline{u}_b(nT_0) &= \sum_{b'=0}^{2N-1} u_{b'b}(nT_0) \\
&= \sum_{\delta b=-b}^{2N-1-b} \mathbf{H}[b] \\
&\quad \sum_{\delta n=-\infty}^{+\infty} a_{b+\delta b}((n+\delta n)T_0)(-1)^{b\delta n} G(\delta n, \delta b). \\
&= \mathbf{H}[b] a_b(nT_0) \\
&\quad + \mathbf{H}[b] \sum_{\delta b \neq 0} \sum_{\delta n=-\infty}^{+\infty} a_{b+\delta b}((n+\delta n)T_0)(-1)^{b\delta n} G(\delta n, \delta b).
\end{aligned} \tag{4.40}$$

The *intrinsic interference* is defined as [17]

$$I(b,n) \triangleq \sum_{\delta b \neq 0} \sum_{\delta n=-\infty}^{+\infty} a_{b+\delta b}((n+\delta n)T_0)(-1)^{\delta bn}(-1)^{b\delta n} G(\delta n, \delta b).$$

From (4.21) it follows

$$Re[I(b,n)] = 0, \quad \forall b, \ \forall n \tag{4.41}$$

In case of ideal channel, i.e. $h(kT) = \delta(kT)$, where $\delta(\cdot)$ is the Kronecker delta, from (4.19) it follows

$$\begin{aligned}
Re[\overline{u}_b(nT_0)] &= \sum_{\delta b=-b}^{2N-1-b} \sum_{\delta n=-\infty}^{+\infty} a_{b+\delta b}((n+\delta n)T_0)(-1)^{b\delta n} Re[G(\delta n, \delta b)]. \\
&= a_b(nT_0).
\end{aligned} \tag{4.42}$$

This means that, in case of ideal channel, a perfect reconstruction of the transmitted signal is obtained. In case of frequency selective channel, instead,

$$\begin{aligned}
Re[\overline{u}_b(nT_0)] &= Re[\mathbf{H}[b]] a_b(nT_0) \\
&\quad - Im[\mathbf{H}[b]] \\
&\quad \sum_{\delta b=-4}^{+4} \sum_{\delta n=-4}^{+4} a_{(b+\delta b \mod 2N)}((n+\delta n)T_0)(-1)^{b\delta n} Im[G(\delta n, \delta b)]
\end{aligned} \tag{4.43}$$

$$\begin{aligned} Im[\overline{u}_b(nT_0)] &= Im[\mathbf{H}[b]]a_b(nT_0) \\ &\quad +Re[\mathbf{H}[b]] \\ &\quad \sum_{\delta b=-4}^{+4}\sum_{\delta n=-4}^{+4} a_{(b+\delta b \mod 2N)}((n+\delta n)T_0)(-1)^{b\delta n}Im[G(\delta n,\delta b)] \end{aligned} \tag{4.44}$$

where limitations on δb and δn are derived from computations reported in Table 4.2.

As far as concerns $\overline{w}_{eq}(kT)$, see (4.31),

$$\overline{w}_{eq}(nT_0) = \sum_k w_{eq}(kT)e^{-j\frac{2\pi}{2N}bk}g(k-nN)e^{-j\varphi_b(nT_0)}. \tag{4.45}$$

By introducing the following definition

$$G_b(\delta n,\delta b) \triangleq (-1)^{b\delta n}G(-\delta n,\delta b), \tag{4.46}$$

from (4.31) and (4.40) it follows

$$\begin{aligned} u_b(nT_0) &= \overline{u}_b(nT_0)+\overline{w}_{eq}(nT_0) \\ &\quad \mathbf{H}[b]\sum_{\delta b} a_{b+\delta b}(n) * G_b(n,\delta b) + \overline{w}_{eq}(nT_0) \end{aligned} \tag{4.47}$$

Relation (4.47) is represented by the scheme shown in Fig. 4.6. Values of $G_b(\delta n,\delta b)$ for b even and odd are reported in Tables 4.3 and 4.4, respectively.

4.2 Active subcarriers computation

In this section the power spectral density (PSD) of $s_u(kT)$ is computed in order to quantify the number of active subcarriers which yields a signal spectrum satisfying mask requirements given in Chapter 3. From Fig. 4.1, the following is derived

$$s_u(kT) = e^{j\frac{2\pi}{2N}bk}\sum_{b\in\mathcal{A}}\sum_{n=-\infty}^{+\infty} a_b(nT_0)e^{j\varphi_b(nT_0)}g((k-nN)T), \tag{4.48}$$

Table 4.3: $G_b(\delta n, \delta b)$ for b even

δn / δb	-4	-3	-2	-1	0	1	2	3	4
-4	0	0	0	j0.002	0	-j0.002	0	0	0
-3	0	0	-j0.002	-j0.01	-j0.018	-j0.01	-j0.002	0	0
-2	0	+j0.002	0	j0.038	0	-j0.038	0	-j0.002	0
-1	-j0.001	-j0.01	-j0.038	-j0.228	-j0.441	-j0.228	-j0.038	-j0.01	-j0.001
0	0	+j0.018	0	+j0.441	1	-j0.441	0	-j0.018	0
1	j0.001	-j0.01	j0.038	-j0.228	j0.441	-j0.228	j0.038	-j0.01	j0.001
2	0	+j0.002	0	+j0.038	0	-j0.038	0	-j0.002	0
3	0	0	j0.002	-j0.01	j0.018	-j0.01	j0.002	0	0
4	0	0	0	+j0.002	0	-j0.002	0	0	0

Table 4.4: $G_b(\delta n, \delta b)$ for b odd

δn / δb	-4	-3	-2	-1	0	1	2	3	4
-4	0	0	0	-j0.002	0	+j0.002	0	0	0
-3	0	0	-j0.002	+j0.01	-j0.018	+j0.01	-j0.002	0	0
-2	0	-j0.002	0	-j0.038	0	+j0.038	0	+j0.002	0
-1	-j0.001	+j0.01	-j0.038	+j0.228	-j0.441	+j0.228	-j0.038	+j0.01	-j0.001
0	0	-j0.018	0	-j0.441	1	+j0.441	0	+j0.018	0
1	j0.001	+j0.01	j0.038	+j0.228	j0.441	+j0.228	j0.038	+j0.01	j0.001
2	0	-j0.002	0	-j0.038	0	+j0.038	0	+j0.002	0
3	0	0	j0.002	+j0.01	j0.018	+j0.01	j0.002	0	0
4	0	0	0	-j0.002	0	+j0.002	0	0	0

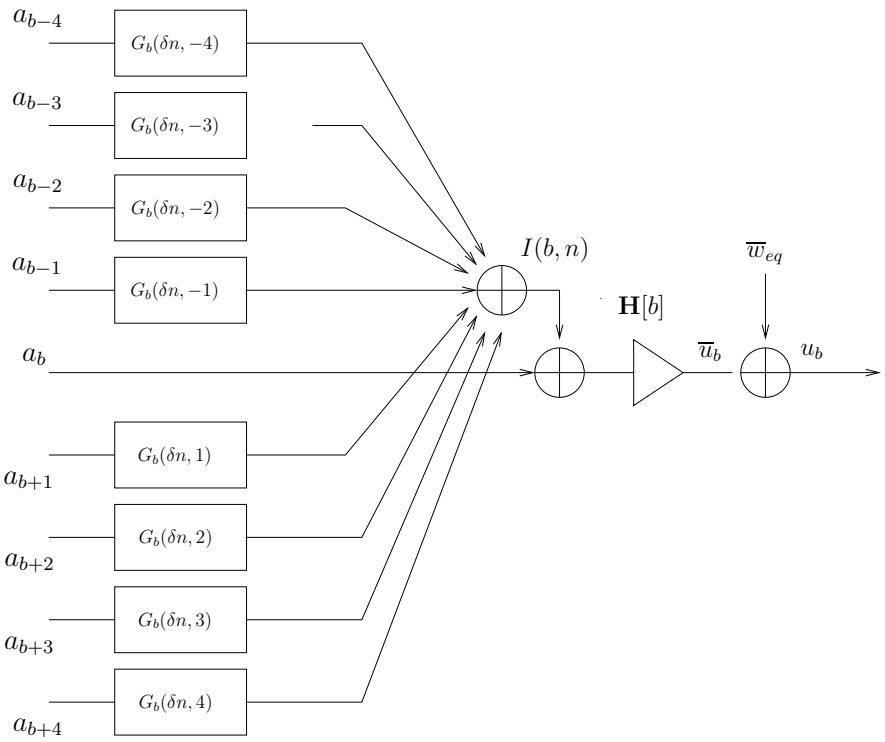

Figure 4.6: Block diagram representing the relation between $u_b(nT_0)$ and $a_{b'}(n'T_0)$, $b' = b-4, \ldots, b+4$.

where $\mathcal{A}$ is defined in (2.2) and the symmetry of $g(kT)$ has been utilized. Hence,

$$\begin{aligned}
\tilde{r}_{s_u}(kT,\tau T) &\triangleq \mathrm{E}[s_u(kT)s_u'((k-\tau)T)] \\
&= \sum_{b_1\in\mathcal{A}}\sum_{b_2\in\mathcal{A}}\sum_{n1}\sum_{n2} e^{j\frac{2\pi}{2N}(b_1k-b_2(k-\tau))}e^{j\varphi_{b_1}(n_1T_0)-\varphi_{b_2}(n_2T_0)} \\
&\qquad g((k-n_1)T)g((k-\tau-n_2)T)\mathrm{E}\left[a_{b_1}(n_1T_0)a_{b_2}(n_2T_0)\right]. \\
&= \frac{\sigma_A^2}{2}\sum_{b\in\mathcal{A}} e^{j\frac{2\pi}{2N}b\tau}\sum_n g((k-nN)T)g((k-\tau-nN)T) \qquad (4.49)
\end{aligned}$$

where (4.10) and (4.11) have been utilized. By a simple variable change, it can be shown that $\tilde{r}_{s_u}(kT,\tau T)$ satisfies

$$\tilde{r}_{s_u}((k+N)T,\tau T) = \tilde{r}_{s_u}(kT,\tau T), \qquad (4.50)$$

namely, $s_u(kT)$ is a cyclostationary random process of period NT. Hence, the average of $\tilde{r}_{s_u}(kT, \tau T)$ is introduced as

$$\begin{aligned} r_{s_u}(\tau T) &= \frac{1}{N}\sum_{k=0}^{N-1}\tilde{r}_{s_u}(kT,\tau T) \\ &= \frac{\sigma_A^2}{2N}\sum_{b\in\mathcal{A}} e^{j\frac{2\pi}{2N}b\tau}c_g(\tau T) \end{aligned} \tag{4.51}$$

where $c_g(\tau T)$ is the deterministic autocorrelation of $g(kT)$ defined as

$$c_g(\tau T) \triangleq \sum_{k=-\infty}^{\infty} g(kT)g((k+\tau)T). \tag{4.52}$$

From (4.20) it follows

$$c_g(\tau T) = \begin{cases} 1 & \text{for } \tau = 0 \\ 0 & \text{for } \tau = n2N, \forall n \text{ integer} \end{cases}. \tag{4.53}$$

Hence, by defining

$$\overline{c}_g(\nu' T_s) = c_g(\nu' 2NT), \tag{4.54}$$

the Fourier transform of $\overline{c}_g(\nu' T_s)$, $\overline{C}_g(f)$ is given by

$$\begin{aligned} \overline{C}_g(f) &= \sum_{\nu'} \overline{c}_g(\nu' T_s) e^{-j\frac{2\pi}{f}\nu' T_s} \\ &= \frac{1}{2N}\sum_{i=0}^{2N-1} C_g\left(f - i\frac{1}{2NT}\right) \\ &= 1, \end{aligned} \tag{4.55}$$

where $C_g(f)$ is the Fourier transform of $c_g(kT)$. Hence, in case of all active subcarriers, the PSD of $s_u(kT)$, defined as

$$R_{s_u}(f) \triangleq \sum_{\tau=-\infty}^{+\infty} r_{s_u}(\tau T) e^{-j2\pi fT}, \tag{4.56}$$

is equal to

$$\begin{aligned} R_{s_u}(f) &= \sigma_A^2 \frac{1}{2N}\sum_{b=0}^{2N-1} C_g\left(f - \frac{1}{2NT}\right) \\ &= \sigma_A^2 \end{aligned} \tag{4.57}$$

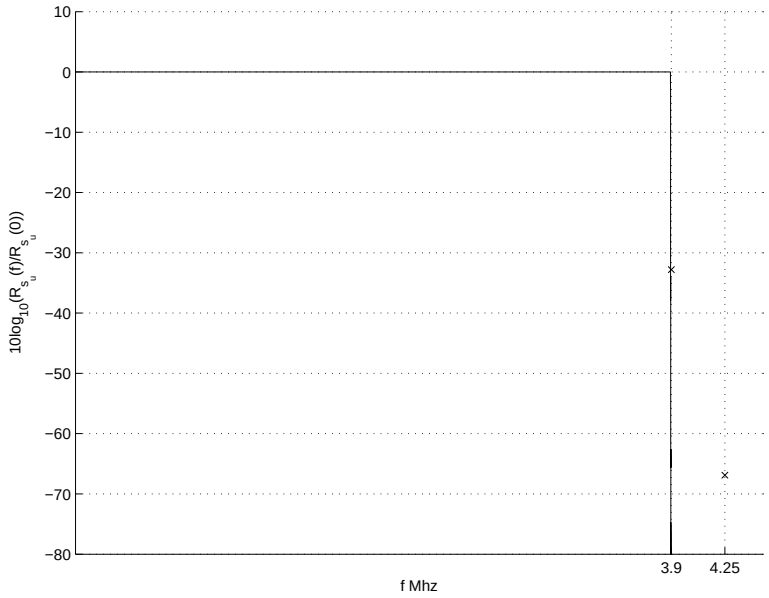

Figure 4.7: Normalized PSD of $s_u(kT)$ in dB and mask constraints at 3.9 and 4.25 Mhz (x markers).

where (4.55) has been utilized. The aim, here, instead, is to determine the number of active subcarriers N_a in order to obtain a transmitted signal whose PSD satisfies the mask constraints. Fig. 4.7 depicts the normalized PSD of $s_u(kT)$ in dB for $N_a = 13950$ and $L = 4M$. In the same figure, mask constraints at 3.9 Mhz and 4.25 Mhz (-32.8 dB and -66.9 dB, respectively) are indicated by x markers. A zoomed view is also depicted in Fig. 4.8. As the figures show, most stringent constraints are satisfied by the choice of $N_a = 13933$.

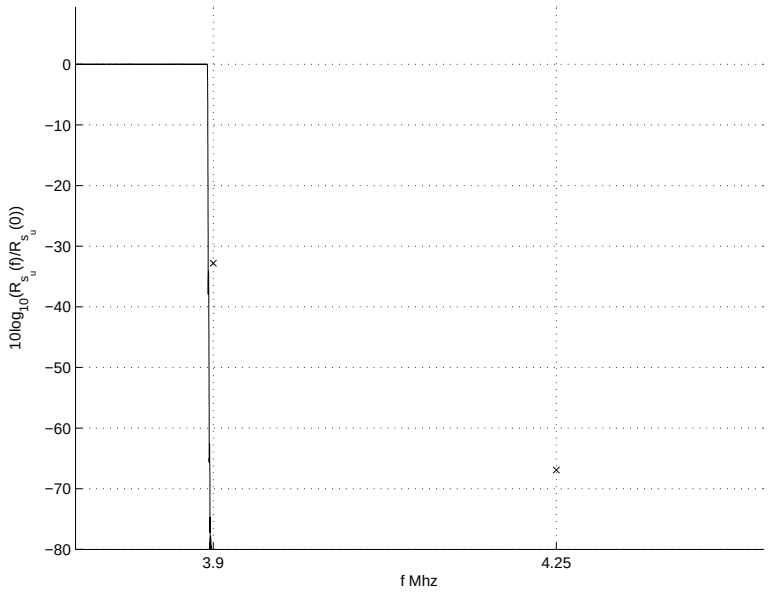

Figure 4.8: Zoomed view of the normalized PSD of $s_u(kT)$ in dB and mask constraints at 3.9 and 4.25 Mhz (x markers).

Chapter 5

Superimposed sequence channel estimation and symbol synchronization

In this chapter channel estimation and synchronization techniques are described. In Fig. 5.1 blocks involved in channel estimation and synchronization are shown. For a comprehensive view refer to Fig. 2.1.

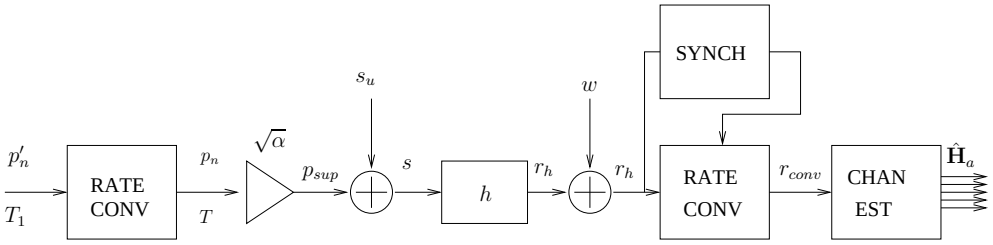

Figure 5.1: Channel estimation and synchronization blocks

5.1 Channel estimation

Channel estimation is based on the superimposed correlation-based method [9]. It consists in superimposing a low power PN sequence to the useful signal, which is exploited at the receiver side to estimate the channel through filtering by

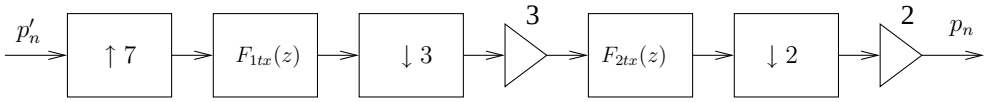

Figure 5.2: Transmitter rate converter.

the matched sequence. The technique has been already studied for the conventional OFDM system [21], but never experimented for OFDM/OQAM based systems. Due to the mask constraints dictated by the DVB-T standard,[26], any PN sequence has to be rate converted, [9], before being transmitted through the channel. Indeed, conventional superimposed correlation method is based on the straightforward superposition of a low power pseudo noise (PN) sequence to the useful transmitted signal and the recovery of the channel values through a filtering by the matched PN sequence. Unfortunately, the white spectrum of the PN sequence may not be able to fulfill realistic spectrum mask constraints, forcing to a rate conversion before the superposition, as is the case of the specifications considered in this work. In the following blocks involved in channel estimation are described.

5.1.1 Rate converters

A low power sequence $p_{sup}(kT)$, superimposed to the useful signal $s_u(k)$ is obtained by the scaling of $p_n(kT)$, which is the result of the rate conversion of a CAZAC PN sequence [9], denoted by $p'_n(kT_1)$. Figs. 5.2 and 5.3 show the functional blocks of transmitter and receiver rate converters, respectively. The PN

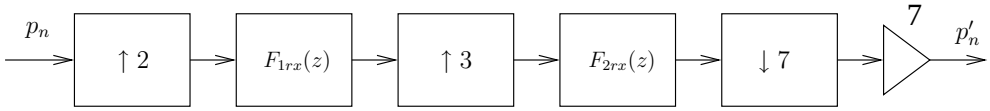

Figure 5.3: Receiver rate converter.

sequence $p'_n(kT_1)$ and the rate converted $p_n(kT)$ are periodic signals whose periods are denoted by $L_{p'_n}$ and L_{p_n}, respectively. The transmitter rate converter has

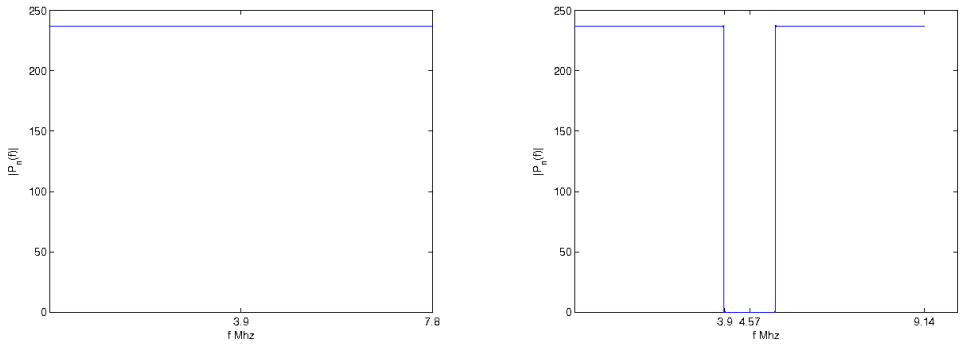

(a) $|P'_n(f)|$ (b) $|P_n(f)|$

Figure 5.4: DFT of the input and output transmitter rate converter.

been designed to obtain a periodic PN sequence $p_n(k)$ with period $L_{p_n} > L_{p'_n}$, whose Discrete Fourier Transform (DFT),

$$P_n\left(K\frac{1}{L_{p_n}T_1}\right) \triangleq \sum_{k=0}^{L_{p_n}-1} p_n(k)e^{-j2\pi\frac{Kk}{L_{p_n}}}, \quad K=0,\ldots,L_{p_n}-1 \tag{5.1}$$

has the same values of the DFT of $p'_n(k)$,

$$P'_n\left(K\frac{1}{L_{p'_n}T}\right) = \sum_{k=0}^{L_{p'_n}-1} p'_n(k)e^{-j2\pi\frac{Kk}{L_{p'_n}}}, \quad K=0,\ldots,L_{p'_n}-1, \tag{5.2}$$

over the unconstrained DVB-T band ($[-3.9Mhz : 3.9Mhz]$), as shown in Fig. 5.4. The aim of the receiver rate converter is to recover $p'_n(k)$. The transmitter rate conversion is performed offline, while receiver circular convolutions can be accomplished via DFT. Fig. 5.5 depicts the transmitter and receiver filters frequency responses in dB, where, according to standard specifications,

$$\frac{1}{2T_1} = 3.9Mhz \quad \text{and} \quad \frac{1}{2T} = 4.57Mhz. \tag{5.3}$$

The choice of $\frac{1}{2T_1} = 3.9Mhz$ is due to the fact that the first and most stringent mask constraint given by the DVB-T standard, [26], is at $3.9Mhz$. In our case $p'_n(kT_1)$ is a periodic pseudonoise CAZAC sequence of period $L_{p'_n} = 56172$ and the resulting rate converted sequence $p_n(kT)$ has period $L_{p_n} = 65534$

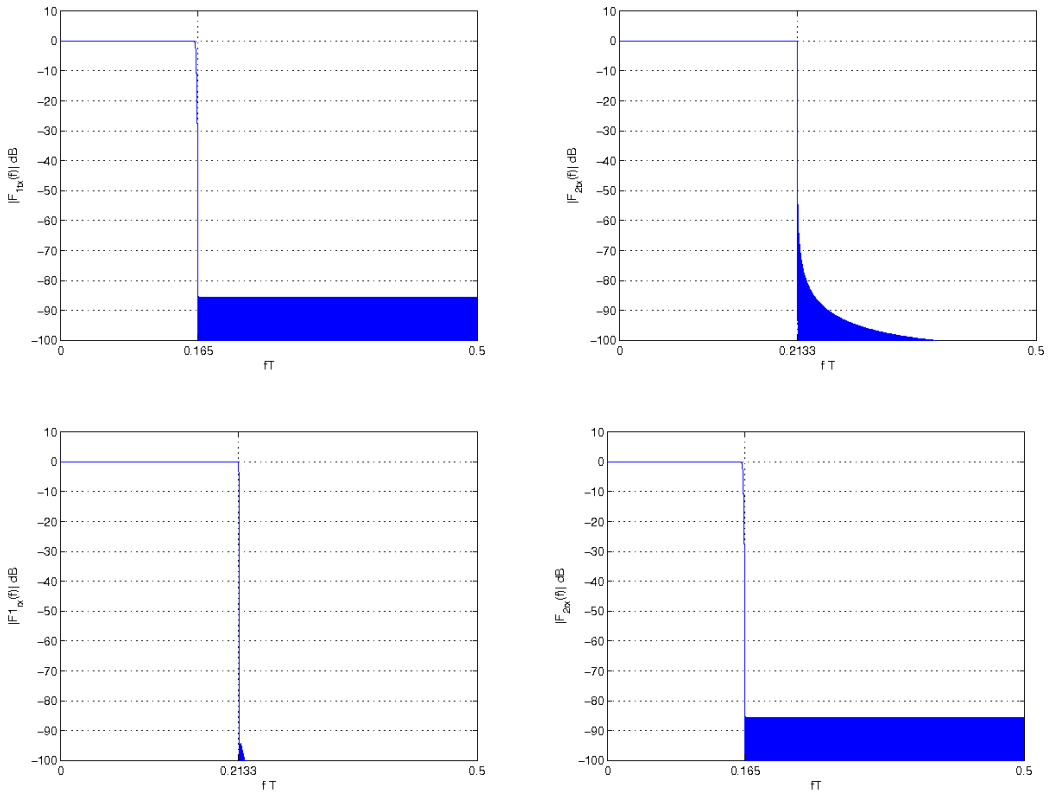

Figure 5.5: Rate converters frequency responses.

5.1.2 Channel estimation module

The basic DVB-T2 transmission unit is the *frame*, [8]. In every frame, N_F OFDM symbols are transmitted, modulating N_a active subcarriers. The modulated signal $s_u(kT)$ contains the beginning of a frame every $N_F M$ samples, where M is the total number of subcarriers. Just before delivering the modulated signal $s_u(kT)$ the filtered and scaled PN sequence $p_{sup}(k)$ is superimposed. Having $p_{sup}(kT)$ and $p_n(kT)$ the same period, a single period of $p_{sup}(kT)$ comprises L_{p_n} samples, corresponding to $T_{p_{sup}} = L_{p_n} T$ seconds. In order to exploit the superimposed sequence also for synchronization purposes, L_{p_n} should be an integer multiple, N_{sup}, of M. Indeed, in such a case the beginning of every period coincides with the beginning of an OFDM symbol. If the condition is not exactly satisfied, the sequence is padded with a small number of zeros before being superimposed as shown in Fig. 5.6. superimpose a signal whose period is an integer multiple N_{sup} of $2N$, a single period is padded with a small number of zeros N_z, as shown in Fig. 5.6. E.g., in our case $M = 16384$, $L_{pn} = 65534$, $N_{sup} = 4$, $N_z = 2$. If the number

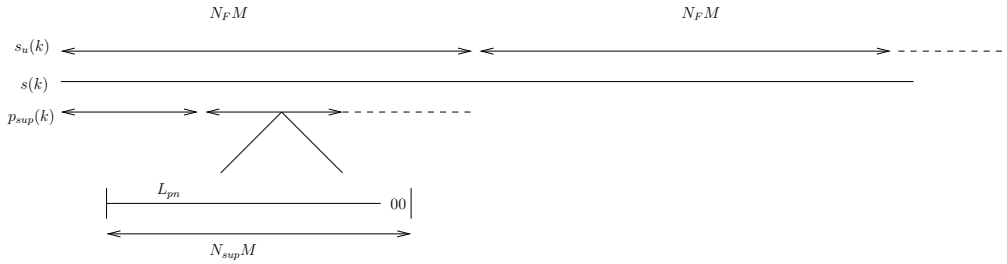

Figure 5.6: Superimposition scheme.

of added zeros is very small with respect to L_{p_n}, as in our case, the estimation operation is not affected . Letting σ^2_{su} be the power of the useful signal, the power level of the superimposed sequence $p_{sup}(k)$ is set to

$$\sigma^2_{p_{sup}} = \beta \sigma^2_{s_u} \tag{5.4}$$

by multiplying $p_n(k)$ by a factor $\sqrt{\alpha}$.

Fig. 5.7 shows the operations performed by the RATE-CONV CHAN-EST block

of Fig. 2.1. The useful signal $s_u(kT)$ and the system noise $w(kT)$ are first neglected since they both play the role of noise as regard channel estimation task. Being $p_{sup}(kT)$ cyclic, $r_h^{(sup)}$ is the cyclic convolution between $p_{sup}(kT)$ and

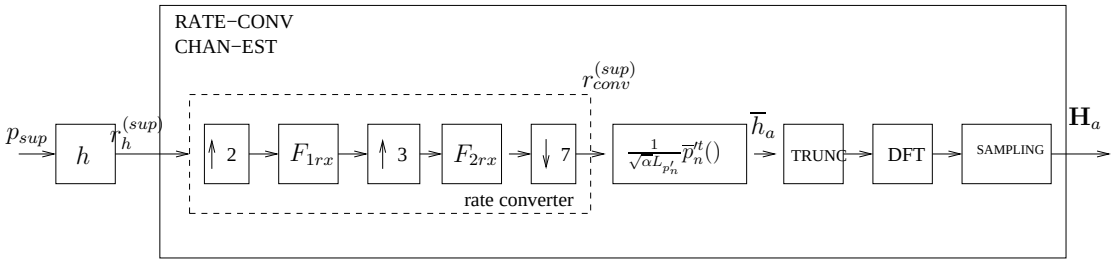

Figure 5.7: Ideal channel estimation module

$h(kT)$. Hence,

$$\begin{aligned} R_h^{(sup)}\left(K\frac{1}{TL_{p_n}}\right) &= \sum_{k=0}^{L_{p_n}-1} r_h^{(sup)} e^{-j2\pi K\frac{1}{TL_{p_n}}kT} \\ &= \sqrt{\alpha}P_n\left(K\frac{1}{TL_{p_n}}\right)H\left(K\frac{1}{TL_{p_n}}\right) \quad K=0,\ldots,L_{p_n}-1. \end{aligned} \tag{5.5}$$

By the property of the rate converter, explained above, the signal at the output of the rate converter $r_{conv}^{(sup)}(kT_1)$, is the cyclic convolution between $p'_n(kT)$ and $\overline{h}_a(kT_1)$, whose Fourier transform is defined as, (2.13)

$$\overline{H}_a(f) = H(f), \quad 0 \le |f| < \frac{F_1}{2}. \tag{5.6}$$

Namely

$$\begin{aligned} R_{conv}^{(sup)}\left(K\frac{1}{T_1L_{p'_n}}\right) &= \sum_{k=0}^{L_{p'_n}-1} r_{conv}^{(sup)}(kT_1) e^{-j2\pi K\frac{1}{T_1L_{p'_n}}kT_1} \\ &= \sqrt{\alpha}P'_n\left(K\frac{1}{T_1L_{p'_n}}\right)H\left(K\frac{1}{T_1L_{p'_n}}\right) \quad K=0,\ldots,L_{p'_n}-1 \\ &= \sqrt{\alpha}P'_n\left(K\frac{1}{T_1L_{p'_n}}\right)\overline{H}_a\left(K\frac{1}{T_1L_{p'_n}}\right) \quad K=0,\ldots,L_{p'_n}-1. \end{aligned} \tag{5.7}$$

Using the following property of the PN sequences

$$p'_n * \overline{p}'^t_n(kT_1) = \begin{cases} L_{p'n} & \text{for} k = NL_{p'_n}, N \text{ integer} \\ 0 & \text{otherwise} \end{cases} \tag{5.8}$$

where $\overline{p}'^t_n$ is the reversed conjugate of $p'^t_n(kT_1)$, defined in (2.6), $\overline{h}_a(kT_1)$ is obtained as

$$\overline{h}_a(kT_1) = \frac{1}{\sqrt{\alpha} L_{p'_n}} r^{(sup)}_{conv} * \overline{p}'^t_n(kT_1), \quad k = 0, \ldots, L_h. \tag{5.9}$$

$\overline{H}_a\left(K \frac{1}{T_1 L_{p'_N}}\right)$ is, then, derived by a DFT over $L_{p'_n}$ samples. Being

$$\frac{1}{T_1 L_{p'_n}} = \frac{1}{T_2 L_p n} = \frac{1}{T_2 N_{sup} M} \tag{5.10}$$

if $\left[-\frac{1}{2T_1} : \frac{1}{2T_1}\right]$ includes the active frequncies set, $\mathbf{H}_a$, defined in (2.14), is derived as follows

$$\mathbf{H}_a[i] = \begin{cases} \overline{H}_a\left(4i \frac{1}{T_1 L_{p'n}}\right) & \text{for } i = 0, \ldots, \lfloor \frac{Na}{2} \rfloor \\ \overline{H}_a\left(\left(L_{p'_n} - 4\left(2\lfloor \frac{N_a}{2} + 1 - i \rfloor\right)\right) \frac{1}{T_1 L_{p'n}}\right) & \text{for } i = \lfloor \frac{N_a}{2} \rfloor + 1, \ldots, N_a - 1 \end{cases} \tag{5.11}$$

represented in Fig. (5.7) by the SAMPLING block. The presence of the useful signal $s_u(kT)$ and the system noise $w(kT)$ prevents from a perfect channel reconstruction, as shown in Fig (5.8). The channel estimate has been denoted by $\hat{\mathbf{H}}_a$.

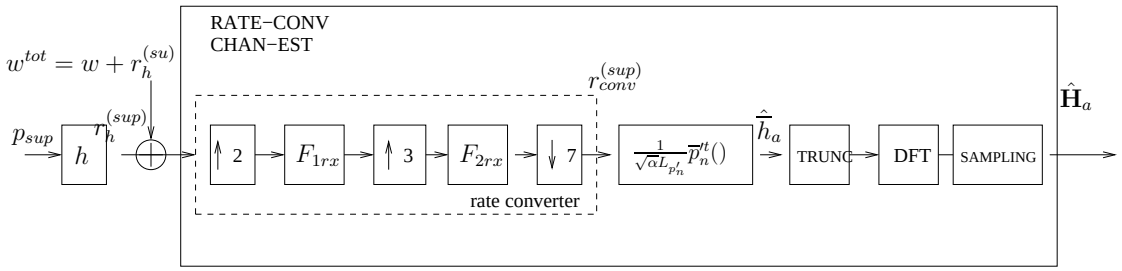

Figure 5.8: Channel estimation module.

Being the rate converter a linear block, its output is given by

$$r_{conv}(kT_1) = r^{(sup)}_{conv}(kT_1) + w^{tot}_{conv}(kT_1) \tag{5.12}$$

where $w_c^{tot}onv$ is the result of the rate conversion of the total noise

$$w^{(tot)}(kT) = w + r_h^{(su)}(kT) \tag{5.13}$$

Hence, an increasing of α lessens the noise contribute, improving the estimation performance. However, at the same time an increasing of α deteriorates the equivalent system SNR defined in (2.11). Results will be given in terms of the parameter β, related to α as follows

$$\alpha\sigma^2_{p_{sup}} = \beta\sigma^2_{s_u}. \tag{5.14}$$

5.2 Synchronization

Before performing any operation, a symbol synchronization is needed. To this aim, the received signal is filtered by the reversed complex conjugate of $p_n^t(k)$. Apart from the system noise and the useful signal, due to the rate conversion, the output of the correlator is not exactly a scaled version of the channel $h(k)$, but something very similar. Hence, the synchronization is performed choosing as reference point the one which achieves the maximum among a slice of L_{p_n} samples at the output of the correlator. E.g., Fig. 5.9, depicts the output of the correlator with the following system settings: $2N = 16384$, $SNR = 7$ dB, 16 QAM constallation, $\beta = 0.08$, $L_{pn} = 65536$, fixed reception channel model, [26]. Dashed vertical lines enclose L_{p_n} wide slices. As the Fig. shows, picks are clearly observable, yielding almost a perfect synchronization on all the checked transmission frame.

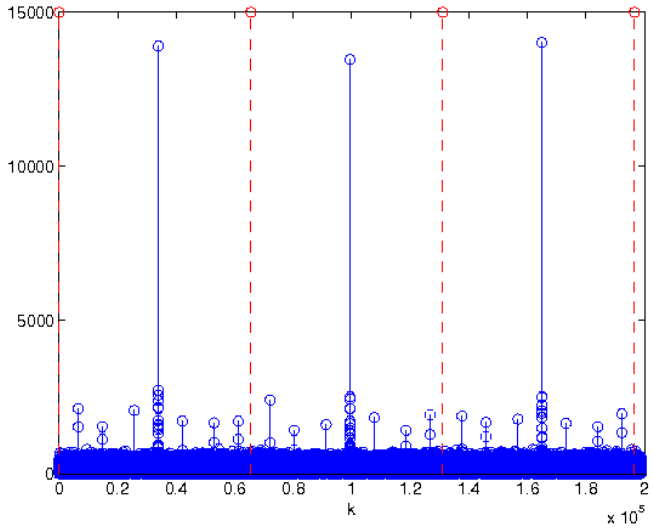

Figure 5.9: Signal at the output of the synchronization correlator.

Chapter 6

Linear Minimum Mean Square Equalization

As shown in Fig. 4.2, OFDM/OQAM system is provided by per branch linear equalizers represented by their zeta transform $C_b(z)$. Fig. 6.1 shows a block diagram representing operations involved in producing the bth output. The equivalent scheme of Fig. 4.6, derived in Chapter 4, has been utilized; $G_b(\delta n, \delta b)$, $b = 0, \ldots, 2N-1$, are defined in (4.46) and their values are reported in Tables 4.3 and 4.4. For each branch b, equalization filter coefficients are computed according to the minimum mean square error criterion (MMSE), namely minimizing

$$MSE \triangleq \mathrm{E}\left[\left|\tilde{A}_b(n'T_s) - A_b(n'T_s)\right|^2\right], \tag{6.1}$$

where $\tilde{A}_b(n'T_s) = \tilde{A}_b^R(n'T_s) + j\tilde{A}_b^I(n'T_s)$ is the received QAM symbol on branch b at instant $n'T_s$ and $A_b(n'T_s)$ the corresponding sent data. In [24] a frequency domain approach has been presented to compute equalization coefficients in case of a prototype filter band limited to $[-\frac{1}{T_s}\ \frac{1}{T_s}]$, which is not the case of $g(kT)$. Here, a time domain approach is used to compute equalization coefficients.

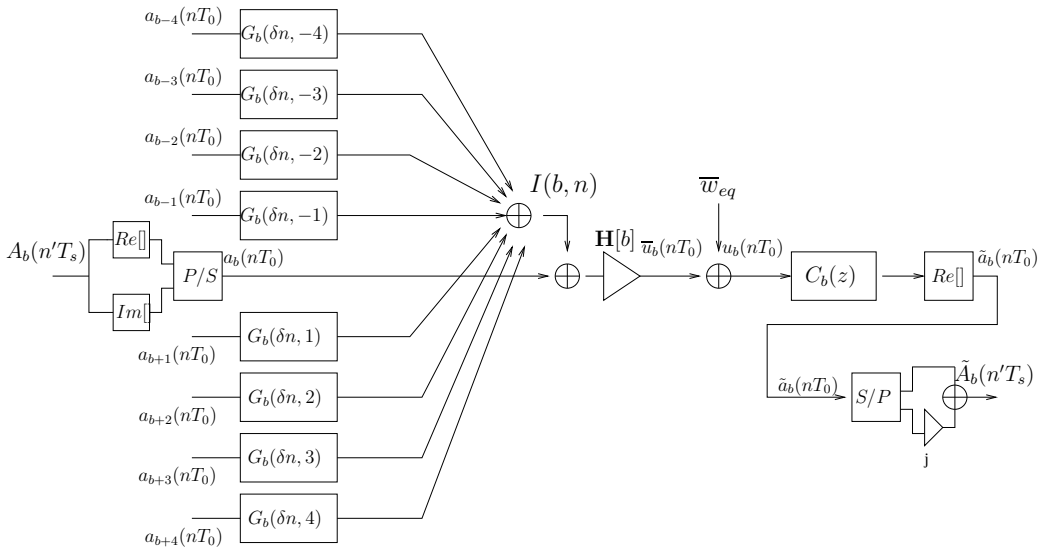

Figure 6.1: Block diagram representing the relation between $u_b(nT_0)$ and $a_{b'}(nT_0)$, $b' = b-4, \ldots, b+4$.

6.1 MSE computation

In the following, for sake of simplicity, the sample period will be omitted, where there's no harm for ambiguity. We suppose equalization filters to have support $[-L_c, L_c]$ and we denote filter coefficients as $c_b(l),\ l = -L_c, \ldots, L_c$. The following vectorial notations are also introduced

$$\begin{aligned}
\mathbf{c}_b &= [c_b(-L_c), \ldots, c_b(L_c)]^T \\
\mathbf{c}_b^R &= [Re[c_b(-L_c)], \ldots, Re[c_b(L_c)]]^T \\
\mathbf{c}_b^I &= [Im[c_b(-L_c)], \ldots, Im[c_b(L_c)]]^T \\
\mathbf{u}_b(n) &= [u_b(n+L_c), \ldots, u_b(n-L_c)]^T \\
\mathbf{u}_b^R(n) &= [Re[u_b(n+L_c)\}, \ldots, \Re\{u_b(n-L_c)]]^T \\
\mathbf{u}_b^I(n) &= [Im[u_b^I(n+L_c)], \ldots, Im[u_b(n-L_c)]]^T
\end{aligned} \tag{6.2}$$

where ^{T} denotes the transpose operator. Denoting by $J_b(\mathbf{c}^R, \mathbf{c}^I)$ the MSE corresponding to the bth branch, from (6.1) and Fig. 6.1 follows

$$\begin{aligned} J_b(\mathbf{c}_b^R, \mathbf{c}_b^I) &= \mathrm{E}\left[\left|\tilde{A}_b(n') - A_b(n')\right|^2\right] \\ &= \mathrm{E}\left[|\tilde{A}_b(n')|^2 + |A_b(n')|^2 - 2Re\{\tilde{A}_b'(n')A_b(n')\}\right] \\ &= \mathrm{E}\left[|A_b(n')|^2\right] + \mathrm{E}\left[\tilde{A}_b^R(n')^2 + \tilde{A}_b^I(n')^2\right] \\ &\quad -2\mathrm{E}\left[A_b^R(n')\tilde{A}_b^R(n') + A_b^I(n')\tilde{A}_b^I(n')\right] \\ &= \mathrm{E}\left[|A_b(n')|^2\right] + \mathrm{E}\left[\tilde{a}_b(2n')^2 + \tilde{a}_b(2n'+1)^2\right] \\ &\quad -2\mathrm{E}\left[a_b^R(2n')\tilde{a}_b(2n') + a_b^I(2n'+1)\tilde{a}_b(2n'+1)\right] \end{aligned} \tag{6.3}$$

Expanding the second term of the summation we have

$$\begin{aligned} &\mathrm{E}\left[\tilde{a}_b(2n')^2 + \tilde{a}_b(2n'+1)^2\right] \\ &= \mathrm{E}\left[Re\{\mathbf{c}_b^T\ \mathbf{u}_b(2n')\}^2 + Re\{\mathbf{c}_b^T\ \mathbf{u}_b(2n'+1)\}^2\right] \\ &= \mathrm{E}\left[(\mathbf{c}_b^{RT}\ \mathbf{u}_b^R(2n') - \mathbf{c}_b^{IT}\ \mathbf{u}_b^I(2n'))^2 + (\mathbf{c}_b^{RT}\ \mathbf{u}_b^R(2n'+1) - \mathbf{c}_b^{IT}\ \mathbf{u}_b^I(2n'+1))^2\right] \\ &= \mathbf{c}_b^{RT}\mathrm{E}\left[\mathbf{u}_b^R(2n')\mathbf{u}^{RT}(2n') + \mathbf{u}_b^R(2n'+1)\mathbf{u}_b^{RT}(2n'+1)\right]\mathbf{c}_b^R \\ &\quad + \mathbf{c}^{IT}\mathrm{E}\left[\mathbf{u}_b^I(2n')\mathbf{u}_b^{IT}(2n') + \mathbf{u}_b^I(2n'+1)\mathbf{u}_b^{IT}(2n'+1)\right]\mathbf{c}_b^I \\ &\quad - \mathbf{c}_b^{RT}\mathrm{E}\left[\mathbf{u}_b^R(2n')\mathbf{u}_b^{IT}(2n') + \mathbf{u}_b^R(2n'+1)\mathbf{u}_b^{IT}(2n'+1)\right]\mathbf{c}_b^I \\ &\quad - \mathbf{c}_b^{IT}\left\{\mathrm{E}\left[\mathbf{u}_b^R(2n')\mathbf{u}_b^{IT}(2n') + \mathbf{u}_b^R(2n'+1)\mathbf{u}_b^{IT}(2n'+1)\right]\right\}^T\mathbf{c}_b^R \end{aligned} \tag{6.4}$$

Introducing the following definitions

$$\begin{aligned} \mathbf{A}_1 &= \mathrm{E}\left[\mathbf{u}_b^R(2n')\mathbf{u}_b^{RT}(2n') + \mathbf{u}_b^R(2n'+1)\mathbf{u}_b^{RT}(2n'+1)\right] \\ \mathbf{A}_2 &= \mathrm{E}\left[\mathbf{u}_b^I(2n')\mathbf{u}_b^{IT}(2n') + \mathbf{u}_b^I(2n'+1)\mathbf{u}_b^{IT}(2n'+1)\right] \\ \mathbf{B} &= -\mathrm{E}\left[\mathbf{u}_b^R(2n')\mathbf{u}_b^{IT}(2n') + \mathbf{u}_b^R(2n'+1)\mathbf{u}_b^{IT}(2n'+1)\right] \end{aligned}$$

(6.4) becomes

$$\begin{aligned} &\mathrm{E}\left[\tilde{a}_b(2n')^2 + \tilde{a}_b(2n'+1)^2\right] \\ &= [\mathbf{c}_b^{RT} \quad \mathbf{c}_b^{IT}]\begin{bmatrix}\mathbf{A}_1 & \mathbf{B} \\ \mathbf{B}^T & \mathbf{A}_2\end{bmatrix}\begin{bmatrix}\mathbf{c}_b^R \\ \mathbf{c}_b^I\end{bmatrix} \end{aligned} \tag{6.5}$$

Note that the matrix

$$\mathbf{R} = \begin{bmatrix} \mathbf{A}_1 & \mathbf{B} \\ \mathbf{B}^T & \mathbf{A}_2 \end{bmatrix} \tag{6.6}$$

is a real valued, positive definte matrix since $\mathrm{E}\left[\tilde{a}_b(2n')^2 + \tilde{a}_b(2n'+1)^2\right] > 0$. About the third term in the summation (6.3)

$$\begin{aligned}
&-2\mathrm{E}\left[a_b^R(2n')\tilde{a}_b(2n') + a_b^I(2n'+1)\tilde{a}_b(2n'+1)\right] \\
&= -2\mathrm{E}\left[a_b^R(2n')Re[\mathbf{c}_b^T\,\mathbf{u}_b(2n')] + a_b^I(2n'+1)Re[\mathbf{c}_b^T\,\mathbf{u}_b(2n'+1)]\right] \\
&= -2\mathrm{E}\Big[a_b^R(2n')(\mathbf{c}_b^{RT}\,\mathbf{u}_b^R(2n') - \mathbf{c}_b^{IT}\,\mathbf{u}_b^I(2n')) \\
&\qquad + a_b^I(2n'+1)(\mathbf{c}_b^{RT}\,\mathbf{u}_b^R(2n'+1) - \mathbf{c}_b^{IT}\,\mathbf{u}_b^I(2n'+1))\Big] \\
&= -2\Big[\mathrm{E}\big[a_b(2n')\mathbf{u}_b^{RT}(2n') + a_b(2n'+1)\mathbf{u}_b^{RT}(2n'+1)\big] \\
&\qquad - \mathrm{E}\big[(a_b(2n')\mathbf{u}_b^{IT}(2n') + a_b(2n'+1)\mathbf{u}_b^{IT}(2n'))\big]\Big] \begin{bmatrix} \mathbf{c}_b^R \\ \mathbf{c}_b^I \end{bmatrix}
\end{aligned} \tag{6.7}$$

Introducing the following definitions,

$$\mathbf{p}_1 \triangleq \mathrm{E}\big[a_b(2n')\mathbf{u}_b^R(2n') + a_b(2n'+1)\mathbf{u}_b^R(2n'+1)\big] \tag{6.8}$$

$$\mathbf{p}_2 \triangleq -\mathrm{E}\big[(a_b(2n')\mathbf{u}_b^I(2n') + a_b(2n'+1)\mathbf{u}_b^I(2n'+1))\big] \tag{6.9}$$

(6.7) becomes

$$-2\mathrm{E}\left[a_b^R(2n')\tilde{a}_b(2n') + a_b^I(2n'+1)\tilde{a}_b(2n'+1)\right] = -2[\mathbf{p}_1^T \quad \mathbf{p}_2^T] \begin{bmatrix} \mathbf{c}_b^R \\ \mathbf{c}_b^I \end{bmatrix}$$

Overall (6.3) can be written as

$$J_b(\mathbf{c}_b^{RT}, \mathbf{c}_b^{IT}) = \mathrm{E}\left[|A_b(n')|^2\right] + [\mathbf{c}_b^{RT} \quad \mathbf{c}_b^{IT}]\mathbf{R}\begin{bmatrix} \mathbf{c}^R \\ \mathbf{c}_b^I \end{bmatrix} - 2[\mathbf{p}_1^T \quad \mathbf{p}_2^T] \begin{bmatrix} \mathbf{c}_b^R \\ \mathbf{c}_b^I \end{bmatrix}. \tag{6.10}$$

Since $J_b(\mathbf{c}_b^{RT}, \mathbf{c}_b^{IT})$ is a quadratic function of $[\mathbf{c}_b^{RT}\ \mathbf{c}_b^{IT}]$ and $\mathbf{R}$ is positive definite, $J_b(\mathbf{c}_b^{RT}, \mathbf{c}_b^{IT})$ is strictly convex and its minimizer is given by

$$\begin{bmatrix} \overline{\mathbf{c}}_b^R \\ \overline{\mathbf{c}}_b^I \end{bmatrix} = \mathbf{R}^{-1} \begin{bmatrix} \mathbf{p}_1 \\ \mathbf{p}_2 \end{bmatrix}.$$

and the corresponding minimum is given by

$$\begin{aligned} J_{min} &= J_b\left(\overline{\mathbf{c}}_b^{RT}, \overline{\mathbf{c}}_b^{IT}\right) \\ &= \sigma_A^2 - \begin{bmatrix}\mathbf{p}_1^T & \mathbf{p}_2^T\end{bmatrix} \mathbf{R} \begin{bmatrix}\mathbf{p}_1 \\ \mathbf{p}_2\end{bmatrix}. \end{aligned} \tag{6.11}$$

6.1.1 Correlation and crosscorrelation functions

By introducing the following autocorrelation and crosscorrelation functions

$$\begin{aligned} \tilde{r}_{u_b}(n,\tau) &= \mathrm{E}\left[u_b(n)u_b^*(n-\tau)\right] \\ \tilde{r}_{u_b^R}(n,\tau) &= \mathrm{E}\left[u_b^R(n)u_b^R(n-\tau)\right] \\ \tilde{r}_{u_b^I}(n,\tau) &= \mathrm{E}\left[u_b^I(n)u_b^I(n-\tau)\right] \\ \tilde{r}_{u_b^R,u_b^I}(n,\tau) &= \mathrm{E}\left[u_b^R(n)u_b^I(n-\tau)\right] \\ \tilde{r}_{a_b,u_b^R}(n,\tau) &= \mathrm{E}\left[a_b(n)u_b^R(n-\tau)\right] \\ \tilde{r}_{a_b,u_b^I}(n,\tau) &= \mathrm{E}\left[a_b(n)u_b^I(n-\tau)\right] \end{aligned}$$

$\mathbf{A}_1$, $\mathbf{A}_2$, $\mathbf{B}$, $\mathbf{p}_1$, $\mathbf{p}_2$, can be written as

$$\mathbf{A}_1 = \begin{bmatrix} \tilde{r}_{u_b^R}(2n'+L_c,0)+\tilde{r}_{u_b^R}(2n'+1+L_c,0) & \cdots & \tilde{r}_{u_b^R}(2n'+L_c,2L_c)+\tilde{r}_{u_b^R}(2n'+1+L_c,2L_c) \\ \vdots & \ddots & \vdots \\ \tilde{r}_{u_b^R}(2n'-L_c,-2L_c)+\tilde{r}_{u_b^R}(2n'+1-L_c,-2L_c) & \cdots & \tilde{r}_{u_b^R}(2n'-L_c,0)+\tilde{r}_{u_b^R}(2n'+1-L_c,0) \end{bmatrix}$$

$$\mathbf{A}_2 = \begin{bmatrix} \tilde{r}_{u_b^I}(2n'+L_c,0)+\tilde{r}_{u_b^I}(2n'+1+L_c,0) & \cdots & \tilde{r}_{u_b^I}(2n'+L_c,2L_c)+\tilde{r}_{u_b^I}(2n'+1+L_c,2L_c) \\ \vdots & \ddots & \vdots \\ \tilde{r}_{u_b^I}(2n'-L_c,-2L_c)+\tilde{r}_{u_b^I}(2n'+1-L_c,-2L_c) & \cdots & \tilde{r}_{u_b^I}(2n'-L_c,0)+\tilde{r}_{u_b^I}(2n'+1-L_c,0) \end{bmatrix}$$

$$\mathbf{B} = \begin{bmatrix} -\tilde{r}_{u_b^R,u_b^I}(2n'+L_c,0)-\tilde{r}_{u_b^R,u_b^I}(2n'+1+L_c,0) & \cdots & -\tilde{r}_{u_b^R,u_b^I}(2n'+L_c,2L_c)-\tilde{r}_{u_b^R,u_b^I}(2n'+1+L_c,2L_c) \\ \vdots & \ddots & \vdots \\ -\tilde{r}_{u_b^R,u_b^I}(2n'-L_c,-2L_c)-\tilde{r}_{u_b^R,u_b^I}(2n'+1-L_c,-2L_c) & \cdots & -\tilde{r}_{u_b^R,u_b^I}(2n'-L_c,0)-\tilde{r}_{u_b^R,u_b^I}(2n'+1-L_c,0) \end{bmatrix}$$

$$\mathbf{p}_1 = \begin{bmatrix} \tilde{r}_{a_b,u_b^R}(2n',-L_c)+\tilde{r}_{a_b,u_b^R}(2n'+1,-L_c) \\ \vdots \\ \tilde{r}_{a_b,u_b^R}(2n',L_c)+\tilde{r}_{a_b,u_b^R}(2n'+1,L_c) \end{bmatrix} \tag{6.12}$$

$$\mathbf{p}_2=\begin{bmatrix} -\tilde{r}_{a_b,u_b^I}(2n',-L_c)-\tilde{r}_{a_b,u_b^I}(2n'+1,-L_c) \\ \vdots \\ -\tilde{r}_{a_b,u_b^I}(2n',L_c)-\tilde{r}_{a_b,u_b^I}(2n'+1,L_c) \end{bmatrix}$$

Since noise and data are assumed to be zero mean and independent, it follows

$$\tilde{r}_{u_b}(n,\tau)=\tilde{r}_{\overline{u}_b}(n,\tau)+\tilde{r}_{\overline{w}_{eq}}(n,\tau). \tag{6.13}$$

$$\tilde{r}_{u_b^R}(n,\tau)=\tilde{r}_{\overline{u}_b^R}(n,\tau)+\tilde{r}_{\overline{w}_{eq}^R}(n,\tau) \tag{6.14}$$

$$\tilde{r}_{u_b^I}(n,\tau)=\tilde{r}_{\overline{u}_b^I}(n,\tau)+\tilde{r}_{\overline{w}_{eq}^I}(n,\tau) \tag{6.15}$$

$$\tilde{r}_{u_b^R,u_b^I}(n,\tau)=\tilde{r}_{\overline{u}_b^R,\overline{u}_b^I}(n,\tau)+\tilde{r}_{\overline{w}^R,\overline{w}_{eq}^I}(n,\tau) \tag{6.16}$$

$$\tilde{r}_{a_b,u_b^R}(n_1,\tau)=\tilde{r}_{a_b,\overline{u}_b^R}(n_1,\tau) \tag{6.17}$$

$$\tilde{r}_{a_b,u_b^I}(n_1,\tau)=\tilde{r}_{a_b,\overline{u}_b^I}(n_1,\tau). \tag{6.18}$$

By introducing

$$\tilde{r}_{\overline{u}_b,\overline{u}_b'}(\tau)=\mathrm{E}\left[\overline{u}_b(n)\overline{u}_b(n-\tau)\right], \tag{6.19}$$

$\tilde{r}_{\overline{u}_b^R}(n,\tau)$, $\tilde{r}_{\overline{u}_b^I}(n,\tau)$, $\tilde{r}_{\overline{u}_b^R,\overline{u}_b^I}(n,\tau)$ can be expressed as

$$\begin{aligned} \tilde{r}_{\overline{u}_b^R}(n,\tau) &= \mathrm{E}\left[\frac{\overline{u}_b(n)+\overline{u}_b'(n)}{2}\frac{\overline{u}_b'(n-\tau)+\overline{u}_b(n-\tau)}{2}\right] \\ &= \frac{1}{4}\left(r_{\overline{u}_b,\overline{u}_b'}(n,\tau)+r'_{\overline{u}_b}(n,\tau)+r_{\overline{u}_b}(n,\tau)+r'_{\overline{u}_b,\overline{u}_b'}(n,\tau)\right) \\ &= \frac{1}{2}\left(Re[r_{\overline{u}_b}(n,\tau)]+Re[r_{\overline{u}_b,\overline{u}_b'}(n,\tau)]\right) \end{aligned} \tag{6.20}$$

$$\begin{aligned} \tilde{r}_{\overline{u}_b^I}(n,\tau) &= \mathrm{E}\left[\frac{\overline{u}_b(n)-\overline{u}_b'(n)}{2j}\frac{\overline{u}_b'(n-\tau)-\overline{u}_b(n-\tau)}{-2j}\right] \\ &= \frac{1}{4}\left(r_{\overline{u}_b}(n,\tau)+r'_{\overline{u}_b}(n,\tau)-r_{\overline{u}_b,\overline{u}_b'}(n,\tau)-r'_{\overline{u}_b,\overline{u}_b'}(n,\tau)\right) \\ &= \frac{1}{2}\left(Re[r_{\overline{u}_b}(n,\tau)]-Re[r_{\overline{u}_b,\overline{u}_b'}(n,\tau)]\right) \end{aligned} \tag{6.21}$$

$$\begin{aligned}\tilde{r}_{\overline{u}_b^R,\overline{u}_b^I}(n,\tau) &= \mathrm{E}\left[\frac{\overline{u}_b(n)+\overline{u}'_b(n)}{2}\frac{\overline{u}'_b(n-\tau)-\overline{u}_b(n-\tau)}{-2j}\right] \\ &= -\frac{1}{4j}\left(r_{\overline{u}_b}(n,\tau)-r'_{\overline{u}_b}(n,\tau)-r_{\overline{u}_b,\overline{u}'_b}(n,\tau)+r'_{\overline{u}_b,\overline{u}'_b}(n,\tau)\right) \\ &= \frac{1}{2}\left(Im[r_{\overline{u}_b,\overline{u}'_b}(n,\tau)]-Im[r_{\overline{u}_b}(n,\tau)]\right).\end{aligned} \tag{6.22}$$

From (4.47) follows

$$\begin{aligned}\tilde{r}_{\overline{u}_b}(n,\tau) &= \mathrm{E}\left[\overline{u}_b(n)\overline{u}'_b(n-\tau)\right] \\ &= |\mathbf{H}[b]|^2\sum_{\delta b_1}\sum_{\delta b_2}\sum_{\delta n_1}\sum_{\delta n_2} r_{a_{b+\delta b_1},a_{b+\delta b_2}}(\tau+\delta n_2-\delta n_1) \\ &\qquad\qquad G_b(\delta n_1,\delta b_1)G'_b(\delta n_2,\delta b_2) \\ &= |\mathbf{H}[b]|^2\sum_{\delta b}\sum_{\delta n} r_{a_{b+\delta b}}(0)G_b(\delta n,\delta b)G'_b(\delta n-\tau,\delta b) \\ &= |\mathbf{H}[b]|^2\frac{\sigma_A^2}{2}\sum_{\delta b}\sum_{\delta n} G_b(\delta n,\delta b)G'_b(\delta n-\tau,\delta b),\end{aligned} \tag{6.23}$$

where (4.10) and (4.11) have been utilized. $\tilde{r}_{\overline{u}_b}(n,\tau)$ doesn't depend on n. Hence, $\overline{u}_b(n)$ is a wide sense stationary process and its correlation can be denoted by

$$r_{\overline{u}_b}(\tau) = \mathrm{E}[\overline{u}_b(n)\overline{u}'_b(n-\tau)]. \tag{6.24}$$

About $\tilde{r}_{\overline{u}_b,\overline{u}'_b}(n)$,

$$\begin{aligned}\tilde{r}_{\overline{u}_b,\overline{u}'_b}(n,\tau) &= \mathrm{E}\left[\overline{u}_b(n)\overline{u}_b(n-\tau)\right] \\ &= \mathbf{H}[b]^2\sum_{\delta b_1}\sum_{\delta b_2}\sum_{\delta n_1}\sum_{\delta n_2} r_{a_{b+\delta b_1},a_{b+\delta b_2}}(\tau+\delta n_2-\delta n_1) \\ &\qquad\qquad G_b(\delta n_1,\delta b_1)G_b(\delta n_2,\delta b_2) \\ &= \mathbf{H}[b]^2\sum_{\delta b}\sum_{\delta n} r_{a_{b+\delta b}}(0)G_b(\delta n,\delta b)G_b(\delta n-\tau,\delta b) \\ &= \mathbf{H}[b]^2\frac{\sigma_A^2}{2}\sum_{\delta b}\sum_{\delta n} G_b(\delta n,\delta b)G_b(\delta n-\tau,\delta b),\end{aligned} \tag{6.25}$$

where (4.10) and (4.11) have been utilized. Since $\tilde{r}_{\overline{u}_b,\overline{u}'_b}(n,\tau)$ doesn't depend on n, the following notation is introduced

$$r_{\overline{u}_b,\overline{u}'_b}(\tau) = \tilde{r}_{\overline{u}_b,\overline{u}'_b}(n,\tau). \tag{6.26}$$

Table 6.1: $\sum_{\delta b} \Lambda_b(\tau, \delta b)$ for $L = 4M$ and b even

τ	-4	-3	-2	-1	0	1	2	3	4
	-0.003	j0.037	0	j0.882	2	-j0.882	0	-j0.037	-0.003

Table 6.2: $\sum_{\delta b} \Lambda_b(\tau, \delta b)$ for $L = 4M$ and b odd

τ	-4	-3	-2	-1	0	1	2	3	4
	-0.003	-j0.037	0	-j0.882	2	j0.882	0	j0.037	-0.003

By defining

$$\Lambda_b(\tau, \delta b) = \sum_{\delta n} G_b(\delta n, \delta b) G'_b(\delta n - \tau, \delta b) \tag{6.27}$$

and

$$\Gamma_b(\tau, \delta b) = \sum_{\delta n} G_b(\delta n, \delta b) G_b(\delta n - \tau, \delta b) \tag{6.28}$$

(6.23) and (6.25) can be written as

$$r_{\overline{u}_b}(\tau) = |\mathbf{H}[b]|^2 \frac{\sigma_A^2}{2} \sum_{\delta b} \Lambda_b(\tau, \delta b) \tag{6.29}$$

and

$$r_{\overline{u}_b, \overline{u}'_b}(\tau) = \mathbf{H}[b]^2 \frac{\sigma_A^2}{2} \sum_{\delta b} \Gamma_b(\tau, \delta b) \tag{6.30}$$

respectively. Values of $\sum_{\delta b} \Lambda_b(\tau, \delta b)$ and $\sum_{\delta b} \Gamma_b(\tau, \delta b)$ for b even and odd are reported in Tables 6.1, 6.2, 6.3 and 6.4, respectively, and values less than 10^{-3} have been approximated to zero. Since values reported in Tables 6.3 and 6.4 are null,

$$r_{\overline{u}_b, \overline{u}'_b}(\tau) = 0, \quad \forall \tau. \tag{6.31}$$

Hence, it follows

$$\begin{aligned} r_{u_b^R}(\tau) &= r_{u_b^I}(\tau) = \frac{1}{2} Re[r_{\overline{u}_b}(\tau)] \\ &= \frac{\sigma_A^2}{4} |\mathbf{H}[b]|^2 Re[\sum_{\delta b} \Lambda_b(\tau, \delta_b)] \end{aligned} \tag{6.32}$$

Table 6.3: $\sum_{\delta b} \Lambda_b(\tau, \delta b)$ for $L = 4M$ and b even

τ	-4	-3	-2	-1	0	1	2	3	4
	0	0	0	0	0	0	0	0	0

Table 6.4: $\sum_{\delta b} \Lambda_b(\tau, \delta b)$ for $L = 4M$ and b odd

τ	-4	-3	-2	-1	0	1	2	3	4
	0	0	0	0	0	0	0	0	0

and

$$\begin{aligned} r_{u_b^R, u_b^I}(\tau) &= -\frac{1}{2} Im[r_{\overline{u}_b}(\tau)] \\ &= -\frac{\sigma_A^2}{4} |\mathbf{H}[b]|^2 Im[\sum_{\delta b} \Lambda_b(\tau, \delta_b)]. \end{aligned} \tag{6.33}$$

About $\tilde{r}_{a_b, \overline{u}_b^R}(n, \tau)$ and $\tilde{r}_{a_b, \overline{u}_b^I}(n, \tau)$ the following holds

$$\begin{aligned} \tilde{r}_{a_b, \overline{u}_b^R}(n, \tau) &= \mathrm{E}[a_b(n) \sum_{\delta b} (-1)^{\delta b(n-\tau)} \sum_{\delta n} a_{b+\delta b}(n - \tau - \delta n) Re[\mathbf{H}[b] G_b(\delta n, \delta b)]] \\ &= \frac{\sigma_A^2}{2} Re[\mathbf{H}[b] G_b(-\tau, 0)]] \\ &= r_{a_b, \overline{u}_b^R}(\tau) \end{aligned} \tag{6.34}$$

and

$$\begin{aligned} \tilde{r}_{a_b, \overline{u}_b^I}(n, \tau) &= \mathrm{E}[a_b(n) \sum_{\delta b} (-1)^{\delta b(n-\tau)} \sum_{\delta n} a_{b+\delta b}(n - \tau - \delta n) Im[\mathbf{H}[b] G_b(\delta n, \delta b)]] \\ &= \frac{\sigma_A^2}{2} Im[\mathbf{H}[b] G_b(-\tau, 0)]] \\ &= r_{a_b, \overline{u}_b^I}(\tau) \end{aligned} \tag{6.35}$$

where (4.10) and (4.11) have been utilized.

From (4.45) follows

$$\begin{aligned} r_{\overline{w}_{eq}}(n,\tau) &= \sum_{k_1}\sum_{k_2} \mathrm{E}[w_{eq}(k_1)w'_{eq}(k_2)]e^{-j\frac{2\pi}{2N}b(k_1-k_2)}e^{-j(\varphi_b(n)-\varphi_b(n-\tau))} \\ &\qquad\qquad g(k_1-nN)g(k_2-(n-\tau)N) \\ &= \sigma^2_{w_eq} j^{-\tau}(-1)^{b\tau}\sum_k g(k)g(k-\tau N) \\ &= \sigma^2_{w_{eq}} G_b(\tau,0) \\ &= r_{\overline{w}_{eq}}(\tau) \end{aligned} \tag{6.36}$$

where definitions (4.12), (4.46) and hypothesis (4.25) have been applied. Since (4.26)–(4.28) imply that $r_{w_{eq},w'_{eq}}(\tau)=0$, it follows that

$$\tilde{r}_{\overline{w}_{eq}\overline{w}'_{eq}}(n,\tau)=0. \tag{6.37}$$

Hence

$$\begin{aligned} r_{\overline{w}^R_{eq}}(\tau) &= r_{\overline{w}^I_{eq}}(\tau) = \frac{1}{2}Re[r_{\overline{w}_{eq}}(\tau)] \\ &= \frac{1}{2}\sigma^2_{w_{eq}} Re[G_b(\tau,0)] \end{aligned} \tag{6.38}$$

$$\begin{aligned} r_{\overline{w}^R_{eq},\overline{w}^I_{eq}}(\tau) &= -\frac{1}{2}Im[r_{\overline{w}_{eq}}(\tau)] \\ &= -\frac{1}{2}\sigma^2_{w_{eq}} Im[G_b(\tau,0)]. \end{aligned} \tag{6.39}$$

Utilizing results derived so far, matrixes (6.13) can be written as

$$\mathbf{A}_1 = \begin{bmatrix} 2r_{u^R_b}(0) & \cdots & 2r_{u^R_b}(2L_c) \\ \vdots & \ddots & \vdots \\ 2r_{u^R_b}(-2L_c) & \cdots & 2r_{u^R_b}(0) \end{bmatrix}$$

$$\mathbf{A}_2 = \begin{bmatrix} 2r_{u^I_b}(0) & \cdots & 2r_{u^I_b}(2L_c) \\ \vdots & \ddots & \vdots \\ 2r_{u^I_b}(-2L_c) & \cdots & 2r_{u^I_b}(0) \end{bmatrix}$$

$$\mathbf{B} = \begin{bmatrix} -2r_{u^R_b,u^I_b}(2n'+L_c,0) & \cdots & -2r_{u^R_b,u^I_b}(2L_c) \\ \vdots & \ddots & \vdots \\ -2r_{u^R_b,u^I_b}(-2L_c) & \cdots & -2r_{u^R_b,u^I_b}(0) \end{bmatrix}$$

$$\mathbf{p}_1 = \begin{bmatrix} 2r_{a_b,u_b^R}(-L_c) \\ \vdots \\ 2r_{a_b,u_b^R}(L_c) \end{bmatrix}$$

$$\mathbf{p}_2 = \begin{bmatrix} -2\tilde{r}_{a_b,u_b^I}(-L_c) \\ \vdots \\ -2r_{a_b,u_b^I}(L_c) \end{bmatrix} \tag{6.40}$$

By using results derived so far and values reported in Tables 4.3, 4.4, 6.3 and 6.4, one tap equalization coefficients are given by

$$\begin{aligned} \begin{bmatrix} \overline{\mathbf{c}}_b^R \\ \overline{\mathbf{c}}_b^I \end{bmatrix} &= \mathbf{R}^{-1} \begin{bmatrix} \mathbf{p}_1 \\ \mathbf{p}_2 \end{bmatrix} \\ &= \begin{bmatrix} \sigma_A^2|\mathbf{H}[b]|^2 + \sigma_{w_{eq}} & 0 \\ 0 & \sigma_A^2|\mathbf{H}[b]|^2 + \sigma_{w_{eq}} \end{bmatrix}^{-1} \begin{bmatrix} \sigma_A^2 Re[\mathbf{H}[b]] \\ \sigma_A^2 Im[\mathbf{H}[b]] \end{bmatrix} \\ &= \begin{bmatrix} \frac{Re[\mathbf{H}[b]]}{|\mathbf{H}[b]]|^2 + \frac{\sigma_{w_{eq}}^2}{\sigma_A^2}} \\ \frac{Im[\mathbf{H}[b]]}{|\mathbf{H}[b]]|^2 + \frac{\sigma_{w_{eq}}^2}{\sigma_A^2}} \end{bmatrix}. \end{aligned} \tag{6.41}$$

Note that for high $\frac{\sigma_A^2}{\sigma_{w_{eq}}^2}$ values, one tap equalization coincides with the ones that can be derived with the zero forcing method. Namely, discarding $\frac{\sigma_A^2}{\sigma_{w_{eq}}^2}$,

$$c_b^R + jc_b^I = \frac{1}{\mathbf{H}[b]} \tag{6.42}$$

where identities

$$\frac{Re[\mathbf{H}[b]]}{|\mathbf{H}[b]]|^2} = Re[\frac{1}{\mathbf{H}[b]}] \tag{6.43}$$

and

$$\frac{Im[\mathbf{H}[b]]}{|\mathbf{H}[b]]|^2} = Im[\frac{1}{\mathbf{H}[b]}] \tag{6.44}$$

have been utilized.

6.2 Noise estimation module

To compute (6.32), (6.33), (6.34), (6.35), (6.38) and (6.39), $\mathbf{H}_a$ and $\sigma^2_{\overline{w}_{eq}}$ are needed. The channel estimate $\hat{\mathbf{H}}_a$ is used instead of $\mathbf{H}_a$. About $\sigma^2_{\overline{w}_{eq}}$, an estimation module has to be introduced in order to achieve the estimate $\hat{\sigma}^2_{\overline{w}_{eq}}$. In Fig. 2.1 the module is indicated as NOISE ESTIMATION. In Fig. 6.2 the computation performed by the module is reported.

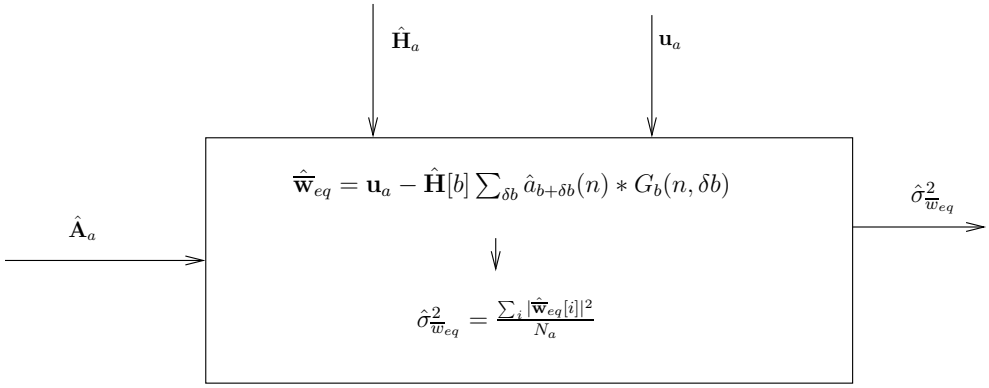

Figure 6.2: Noise estimation module.

$\hat{\mathbf{A}}_a$ is the vector of symbols obtained by re-encoding and re-mapping the decoded output bitstream, while $\hat{\mathbf{H}}_a$ is yielded by the channel estimation module. Note that, in case of perfect channel and symbol knowledge, form (4.47) follows

$$\overline{\mathbf{w}}_{eq} = \mathbf{u}_a - \mathbf{H}[b] \sum_{\delta b} a_{b+\delta b}(n) * G_b(n, \delta b). \tag{6.45}$$

Chapter 7

Results and conclusions

In this chapter main system parameters are summarized, simulation results are reported and conclusions are drawn.

7.1 Simulation results

All blocks reported in Fig. 2.1 have been implemented, according to the description given in the previous chapters and the specifications summarized in Table 7.1. Specifications regarding OFDM-CD3 are also reported. Coding specifications are reported in Table 7.2. For LDPC coding and decoding tasks, functions by the open source Iterative Solutions Coded Modulation Library (ISCML), [30], have been used.

Three constellation sizes have been addressed, namely 16 QAM, 64 QAM and 256 QAM. For each of them, the next generation DVB-T standard provides specific interleaver and demultipexing patterns [8]. The system noise has been modeled as a circularly symmetric gaussian random process, whose power is denoted as σ_w^2. Equalization is accomplished by one tap equalizer for both systems.

We define the bit error rate (BER) as the transmission rate which gives an error probability of 10^{-6} or less divided by the bandwidth occupied. By simulation results, β values have been found for each constellation size in order to minimize

	OQAM	OFDM-CD3
Total subcarriers ($2N$)	16384	16384
Active subcarriers (N_a)	13933	13921
Virtual subcarriers (N_V)	343	1375
Cyclic prefix fraction (Δ)		$\frac{1}{8}$
Channel model	fixed reception cahnnel (F1)	fixed reception channel (F1)
Sampling period (T)	$\frac{7}{64}\,\mu s$	$\frac{7}{64}\,\mu s$
Prototype filter length L_g	4N	
p'_n length ($L_{p'_n}$)	56172	
p_n length (L_{p_n})	65534	
OFDM symbols per frame N_F	100	107 (16-256 QAM) 119 (64QAM)
DVB-T channel bandwidth	8 Mhz	8 Mhz
Codewords per frame 16-64-256 QAM	86-129-172	91-152-182

Table 7.1: Specifications for OQAM and OFDM-CD3 systems.

LDPC code rate	$K_{bch}(=N_u)$	k_{ldpc}	BCH t-correction	$N_{bch}-K_{bch}$	n_{ldpc}
$\frac{1}{2}$	32208	32400	12	192	64800

Table 7.2: Coding sepcifications.

the BER . Increasing β has two main consequences: decreasing the channel estimation MSE and reducing the equivalent SNR, $\sigma^2_{s_u}/\sigma^2_w$. Hence, it is worthwhile increasing β only if through channel estimation improvement we recover effects of SNR worsening. The following values have been found: $\beta = 0.08$ for 16 QAM, $\beta = 0.1$ for 64 QAM, $\beta = 0.3$ for 256 QAM. Figs. 7.1, 7.2, 7.3 depict systems BER versus SNR for 16, 64 and 256 QAM, respectively. As shown, for 16 QAM and 64 QAM, to achieve the target bit error rate, almost the same SNR is required for both systems, namely about 7.4 dB and 12.1 dB, respectively. For 256 QAM, instead, OQAM system requires an SNR 0.5 dB higher than the one required by OFDM-CD3, given by $\Lambda = 16.5$ dB. From the latter results and the specifications given in the previous Tables, curves depicted in Fig. 7.4 and 7.5 are derived. Fig. 7.4 depicts the transmission rate in $Mbps$ versus SNR: 15.46, 23.18, 3.91 Mbps for OFDM/OQAM and 13.59, 20.4, 27.17 for OFDM-CD3. Corresponding spectral efficiencies, in bps/Hz versus SNR, are reported in Fig. 7.5.
OFDM/OQAM system clearly outperforms OFDM-CD3, yielding transmission rates more then 13% higher for all SNR. Namely, improvements of 1.87 Mbps,2.78 Mbps, 3.74 Mbps are achieved at about 7, 12, 17 dB. Moreover, at the same SNR, perfect synchronization for all the constellations is achieved.

7.2 Conclusions

In this work a OQAM based system for the next generation DVB-T standard has been proposed and its performance, in terms of spectral efficiency, has been compared to OFDM-CD3 performancce. As far as concern coding, LDPC and BCH codes have been utilized, synchronization and channel estimation have been performed by a superimposed technique and a one tap MMSE equalization scheme has been adopted. As showed by simulation results, an improvement of more than 13% is achieved by OFDM/OQAM system, confirming, in a practical system, the expectation of a significant spectral efficiency improvement.

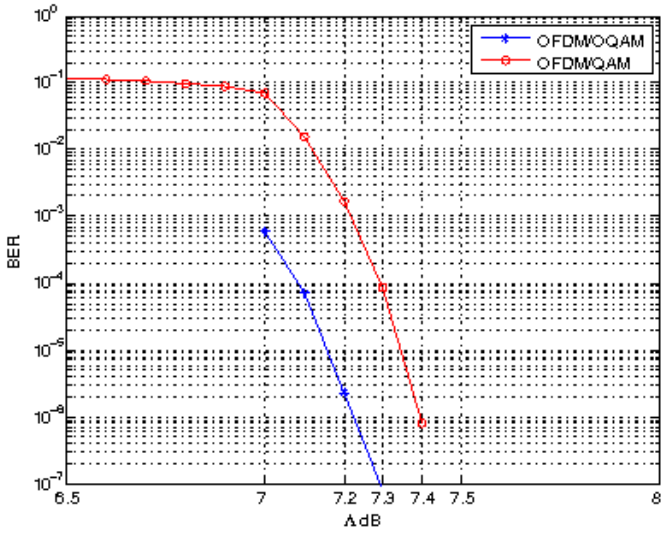

Figure 7.1: BER of 16 QAM OQAM and OFDM-CD3 systems

.

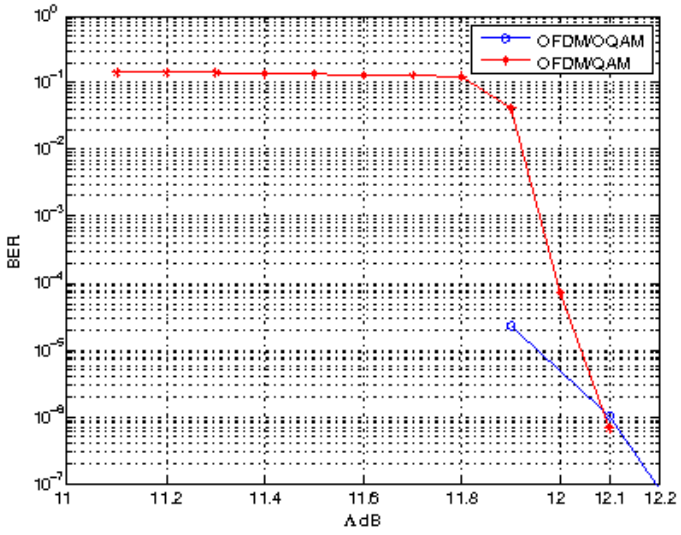

Figure 7.2: BER of 64 QAM OQAM and OFDM-CD3 systems.

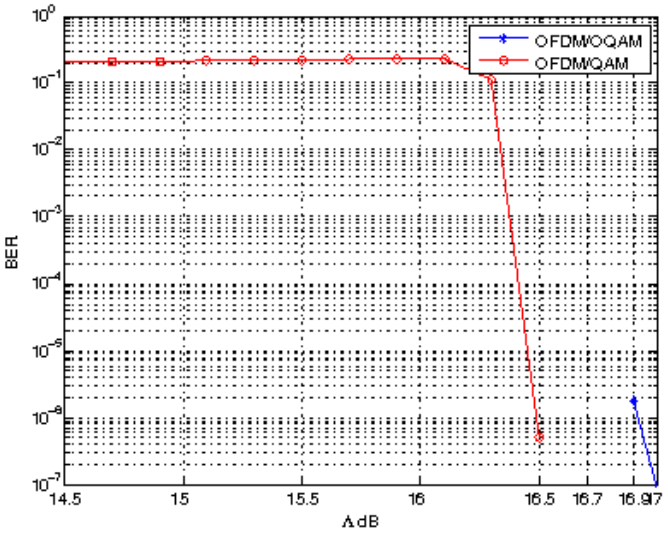

Figure 7.3: BER of 256 QAM OQAM and OFDM-CD3 systems

.

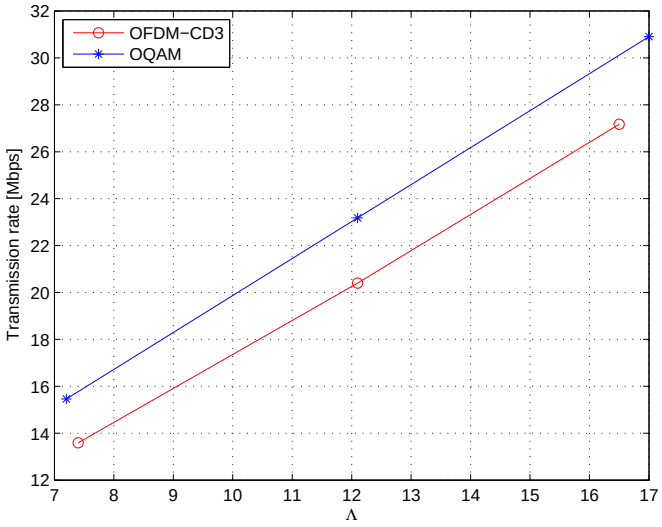

Figure 7.4: Transmission rates of OQAM and OFDM-CD3 systems.

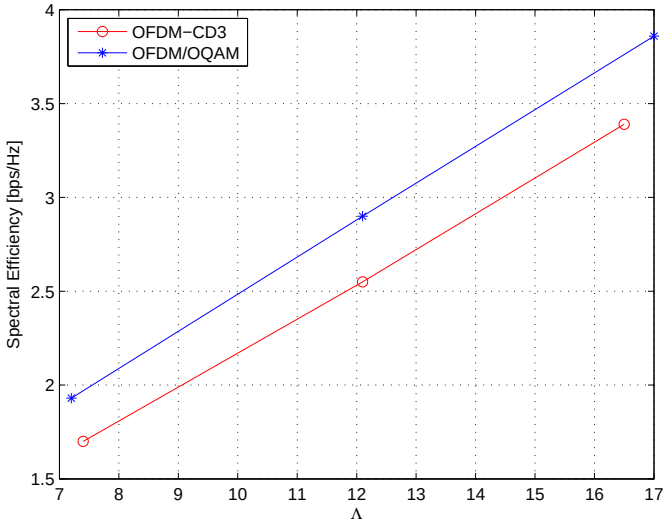

Figure 7.5: Spectral efficiencies of OQAM and OFDM-CD3 systems.

Bibliography

[1] B. Floch, M. Alard, and C. Berrou, "Coded orthogonal frequency division multiplex," *IEEE Transactions on Signal Processing*, vol. 48, no. 11, pp. 3052–3061, May 2000. 15, 17, 18

[2] C. Dosch, P. Ratliff, and D. Pommier, "First public demonstration of COFDM/MASCAM: a milestone for the future of radio broadcasting," *EBU Rev.–Tech., no. 232*, Dec. 1988. 15

[3] DVB. [Online]. Available: http://www.dvb.org 15, 45, 47

[4] *Digital Video Broadcasting (DVB); framing structure, channel coding and modulation for 11/12 GHz satellite service*, ETSI Std. EN 300 421, 1993. 15

[5] *Digital Video Broadcasting (DVB); framing structure, channel coding and modulation for cable systems*, ETSI Std. EN 300 429, 1994. 15

[6] *Digital broadcasting systems for television, sound and data services; framing structure, channel coding and modulation for digital terrestrial television*, ETSI Std. EN 300 744, 1997. 16

[7] *Digital Video Broadcasting (DVB); Second generation framing structure, channel coding and modulation systems for Broadcasting, Interactive Services, News Gathering and other broadband satellite applications)*, ETSI Std. EN 302 307, 2005. 16

[8] A122: Framing structure, channel coding and modulation for a second generation digital terrestrial television broadcasting system (DVB-T2). [Online]. Available: http://www.dvb.org/technology/dvbt2/ 16, 20, 26, 33, 35, 39, 42, 43, 72, 89

[9] N. Benvenuto and G. Cherubini, *Algorithms for Communications Systems and their Applications*. Chichester: John Wiley and Sons Ltd, 2002. 17, 19, 25, 27, 68, 69

[10] R. Chang, "High-speed multichannel data transmission with band limited orthogonal signal," *Bell Syst. Tech. J.*, vol. 45, no. 6, pp. 1775–1796, Dec. 1966. 17

[11] B. R. SALTZBERG, "Performance of an efficient parallel data transmission system," *IEEE Transactions on Communication Technology*, vol. COM-15, pp. 805–811, Dec. 1967. 17

[12] B. Hirosaki, "An orthogonally multiplexed qam system using the discrete fourier transform," *IEEE Transactions on Communications*, vol. COM-29, no. 1, pp. 982–989, Jan. 1981. 17

[13] G.Cariolaro and F.C.Vagliani, "An OFDM Scheme with a Half Complexity," *IEEE Journal on Selected Areas in Communications*, vol. 13, pp. 1586–1599, Dec. 1995. 17

[14] P. Siohan, C. Siclet, and N. Lacaille, "Analysis and design of OFDM/OQAM systems based on filterbank theory," *IEEE Transactions on Signal Processing*, vol. 50, pp. 1170–1183, May 2002. 17, 18, 53, 54

[15] C. Roche and P. Siohan, "A family of extended gaussian functions with a nearly optimal localization property," in *Proc. First Int. Workshop Multi-Carrier Spread-Spectrum*, Oberpfaffenhofen, Germany, Apr. 1997, pp. 179–186. 18

[16] P. Siohan and C. Roche, "Cosine-modulated filterbanks based on extended gaussian functions," *IEEE Transactions on Signal Processing*, vol. 48, no. 11, pp. 3052–3061, May 2000. 18, 53, 54

[17] J. P. Javaudin, D. Lacroix, and A. Rouxle, "Pilot-aided channel estimation for OFDM/OQAM," in *Proc. VTC'03*, vol. 3, Jeju Island, Korea, Apr. 2003, pp. 1581–1585. 18, 19, 61

[18] D.Lacroix-Penther and J.-P. Javaudin, "A new channel estimation method for OFDM/OQAM," in *Proc. of the 7th International OFDM workshop*, Sept. 2002. 19

[19] C. Lele, P. Siohan, R. Legouable, and J. P. Javaudin, "Preamble-based channel estimation techniques for OFDM/OQAM over the powerline," in *Proc. ISPLC'07*, vol. 3, Pisa, Italy, Mar. 2007, pp. 59–64. 19

[20] C. Lele, P. Siohan, and R. Legouable, "2 db better than cp-ofdm with OFDM/OQAM for preamble-based channel estimation," in *Proc. ICC'08*, Beijing, China, May 2008, pp. 1302–1306. 19

[21] A. Goljahani, N. Benvenuto, S. Tomasin, and L. Vangelista, "A superimposed periodic pilot scheme for semi-blind channel estimation of OFDM systems," in *Proc. WPMC'07*, Jaipur, India, Dec 2007. 19, 69

[22] B. Jahan, M. Lanoiselee, G. Degoulet, and R. Rabineau, "Full synchronization method for OFDM/OQAM and ofdm/qam modulations," in *Proc. ISSSTA'08*, Bologna, Itlay, Aug. 2008, pp. 344–348. 19

[23] H. Lin, C. Lelé, and P. Siohan, "Equalization with interference cancellation for hermitian symmetric OFDM/OQAM systems," in *Proc. ISPLC'08*, Jeju Island, Korea, Apr. 2008, pp. 363–368. 20

[24] G. Lin, L. Lundheim, and N. Holte, "On efficient equalization for ofdm/oqam systems," Department of Telecommunications Norwegian University of Science and Technology (NTNU), 7491 Trondheim, Norway, Tech. Rep. DEC-TR-506, Jul. 2005. 20, 22, 77

[25] V. Mignone, A. Morello, and M. Visentin, "Cd3-ofdm: a new channel estimation method to improve the spectrum efficiency in digital terrestrial television systems," in *Proc. IBC'95*, vol. 2, Amsterdam, Sept. 1995, pp. 122–128. 20, 21, 30, 32, 34

[26] *Digital Video Broadcasting (DVB); Framing structure, channel coding and modulation for digital terrestrial television*, ETSI Std. EN 300 744 V1.5.1, 2004-2006. 25, 39, 69, 70, 75

[27] S. B. WEINSTEIN and P. M. EBERT, "Data transmission by frequency-division multiplexing using the discrete fourier transform," *IEEE Transactions on Communication Technology*, vol. COM-19, pp. 628–634, Oct. 1971. 30

[28] P. de Bot, B. L. Floch, V. Mignone, and H. Schutte, "An overview of the modulation and channel coding schemes developed for digital terrestrial television broadcasting within the dttb project," in *Proc. IBC'94*, Amsterdam, 1994. 34

[29] M. Alard, C. Roche, and P. Siohan, "A new family of functions with a nearly optimal time-frequency localization (draft)," Wavecom (Alard) - CNET/DMR, France Telecom Group (Roche and Siohan), Wavecom: Issy-Les Moulineaux, France- CNET/DMR, France Telecom Group: Cesson-Sévigné Cedex, France, Tech. Rep., May 1999. 49

[30] (2007) Iterative solutions. [Online]. Available: http://www.iterativesolutions.com/ 89